The human placenta shapes the phenotype of decidual macrophages.

Sigrid Vondra[1§], Anna-Lena Höbler[1$], Andreas Ian Lackner[1], Johanna Raffetseder[2], Zala Nikita Mihalic[3], Andrea Vogel[4,5], Leila Saleh[6], Victoria Kunihs[6], Peter Haslinger[1], Markus Wahrmann[7], Heinrich Husslein[8], Raimund Oberle[9], Julia Kargl[3], Sandra Haider[4], Paulina Latos[10], Gernot Schabbauer[4,5], Martin Knöfler[4], Jan Ernerudh[11], Jürgen Pollheimer[1*]

[1]Department of Obstetrics and Gynecology, Reproductive Biology Unit, Maternal-fetal Immunology Group, Medical University of Vienna, Austria. [2]Division of Inflammation and Infection (II), Department of Biomedical and Clinical Sciences (BKV), Linköping University, Linköping, Sweden. [3]Otto Loewi Research Center, Division of Pharmacology, Medical University of Graz, Austria. [4]Institute for Vascular Biology, Centre for Physiology and Pharmacology, Medical University Vienna, Austria. [5]Christian Doppler Laboratory for Arginine Metabolism in Rheumatoid Arthritis and Multiple Sclerosis, Vienna, Austria. [6]Department of Obstetrics and Gynecology, Reproductive Biology Unit, Placental Development Group, Medical University of Vienna, Austria. [7]Division of Nephrology and Dialysis, Department of Medicine III, Medical University of Vienna, Vienna, Austria. [8]Department of Obstetrics and Gynecology, Medical University of Vienna, Vienna, Austria. [9]Center for Pathobiochemistry and Genetics, Institute of Medical Chemistry, Medical University of Vienna, Austria. [10]Center for Anatomy and Cell Biology, Medical University of Vienna, Austria. [11]Department of Clinical Immunology and Transfusion Medicine, Department of Biomedical and Clinical Sciences, Linköping University, Linköping, Sweden.

Short title: The placenta induces decidual macrophages

§ These authors contributed equally to this work

* Correspondence to Jürgen Pollheimer: juergen.pollheimer@muv.ac.at

Abstract

During human pregnancy, placenta-derived extravillous trophoblasts (EVT) invade the decidua and communicate with maternal immune cells. The decidua can be distinguished into basalis (decB) and parietalis (decP), the latter being unaffected by placentation. By defining a novel gating strategy, we report accumulation of myeloid cells in decB. We identified a decidua basalis-associated macrophage (decBAM) population with a differential transcriptome and secretome when compared to decidua parietalis-associated macrophages (decPAMs). decBAMs are CD11c^{hi} and efficient inducers of Tregs, proliferate *in situ* and secrete high levels of CXCL1, CXCL5, M-CSF, and IL-10. In contrast, decPAMs exert a dendritic cell-like, motile phenotype characterized by induced expression of HLA class II molecules, enhanced phagocytosis, and the ability to activate T cells. Strikingly, EVT-conditioned media are able to convert decPAMs into a decBAM phenotype. Cumulatively, these findings assign distinct macrophage phenotypes to decidual areas depending on placentation and further highlight a critical role for EVTs in the induction of pregnancy-tolerant macrophage polarization.

Graphical Abstract

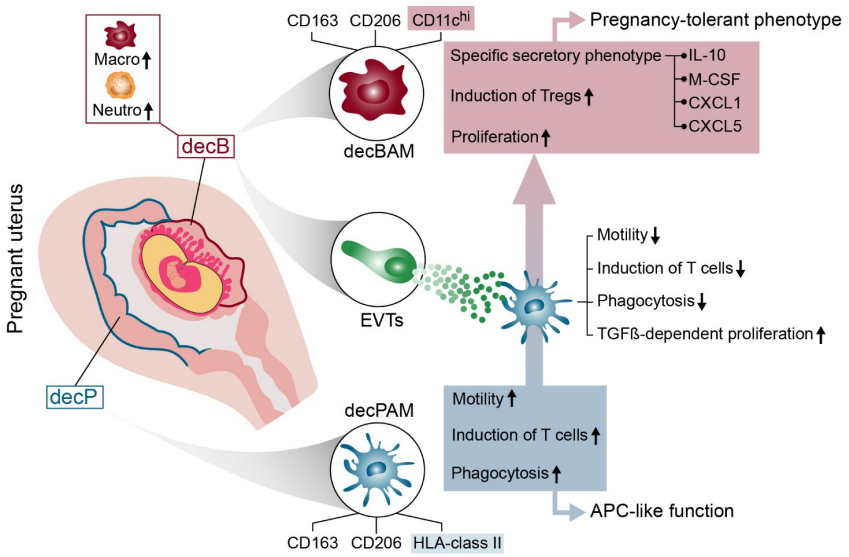

Highlights: In this study, we identified so far unrecognized, placenta-induced immune responses at the maternal-fetal interface. Altogether, we imply that placenta-derived trophoblasts induce a pregnancy-tolerant phenotype by suppressing antigen-presenting cell-like functions in maternal tissue macrophages.

50 **Introduction**

51 During human pregnancy, fetal-derived placental extravillous trophoblasts (EVTs) invade the
52 decidualized mucosal uterine surface, referred to as decidua (Knofler et al., 2019). This unique
53 process, in which semi-allogeneic EVTs intermingle and communicate with maternal decidual
54 immune cells, is fundamental for the maintenance and success of pregnancy. An imbalance in
55 these interactions can lead to the development of obstetrical syndromes such as preeclampsia
56 or uterine growth restriction (Brosens et al., 2011). The human decidua has been the subject
57 of various studies directed towards understanding the function of uterine immune cell types.
58 Under physiological conditions, the maternal-fetal interface is dominated by a non-cytotoxic
59 immune cell response, which enables fetal tolerance and supports placental function
60 (Erlebacher, 2013; Moffett et al., 2017). A central role in the maintenance of this tissue-specific,
61 pregnancy-sustaining environment has been assigned to an interactive network between EVTs
62 and maternal immune cells. Remarkably, decidual natural killer (dNK) cells and macrophages
63 cooperate to transform the decidual vasculature into dilated conduits able to deliver high
64 amounts of low-pressure blood to the growing fetus (Pollheimer et al., 2018). Genetic data
65 suggest that the specific combination of killer-cell immunoglobulin-like receptors expressed on
66 dNK cells and their MHC ligands on EVTs are crucial in determining reproductive success
67 (Hiby et al., 2010). Moreover, there are also indications for an active suppression of immune
68 responses at the maternal-fetal interface. In humans, EVTs have been demonstrated to induce
69 a non-cytotoxic phenotype in dNK cells by initiating intercellular trafficking of the non-classical
70 MHC-I class molecule HLA-G (Tilburgs et al., 2015). In addition, studies in mice suggest an
71 active blockage of T cell infiltration at the maternal-fetal interface even after forced reactivation
72 of maternal memory T cells by placenta-specific overexpression of ovalbumin (Nancy et al.,
73 2012). However, little is known about the specific function of decidual macrophages. A previous
74 paper reported two distinct macrophage populations expressing either high or low levels of cell
75 surface CD11c. The authors further suggested that the CD11c^{lo} population comprise an
76 antigen-presenting cell (APC) population (Houser et al., 2011). Recently, a single-cell
77 transcriptomic approach identified various maternal macrophage subpopulations in the human

78 decidua, two of which constitute tissue resident cells, referred to as dM1 and dM2, and one is
79 found in the intervillous space adhering to placental villi, designated as dM3 (Vento-Tormo et
80 al., 2018). The dM3 type was recently characterized and identified as placenta-associated
81 maternal macrophages (PAMMs) (Thomas et al., 2021). In this paper, the authors also
82 unraveled distinctive phenotypes of fetal-derived placental macrophages, referred to as
83 Hofbauer cells (HB). Different to HBs and PAMMs in the intervillous space, decidual tissue-
84 resident macrophages are not uniformly confronted with placental tissues. After the blastocyst
85 becomes embedded in the endometrium and the placenta develops, the formation of the
86 maternal-fetal interface occurs only at a specific uterine site, the decidua basalis (decB). In
87 contrast, large areas of the decidua, the decidua parietalis (decP), are unaffected by
88 placentation. While various morphological differences such as degree of vascularization
89 (Plaisier et al., 2007; Windsperger et al., 2020) or tissue stiffness (Abbas et al., 2019) have
90 been noticed, little is known about the difference between decB and decP tissues in terms of
91 immune cell content and activation. In a recent publication, we were able to show low
92 abundance of T cells in decB tissues when compared to decP samples. The drop in both $CD4^+$
93 helper and $CD8^+$ cytotoxic T cells was further associated with low abundance of T cell-
94 recruiting high endothelial venules (Windsperger *et al.*, 2020). These findings imply
95 fundamental differences in immune cell distribution and extravasation into decB and decP.
96 However, to date, there are no comparative data on immune cell distribution or function in
97 decB and decP tissues that allow conclusions to be drawn about placentation-dependent
98 effects on decidual immune cells.
99 In this study, we set out to select donor-matched first-trimester decB and decP tissue samples
100 in order to identify immunological adaptation that specifically occur in response to placentation.
101 By defining a novel flow cytometry gating strategy, we demonstrate that tissue-resident
102 macrophages and neutrophils accumulate in decB tissues. We further identified a specific
103 phenotype and functionality of decB-associated macrophages (decBAMs) in comparison to
104 decP-associated macrophages (decPAMs). While decBAMs show a higher capacity to

105 proliferate and induce Treg formation, decPAMs are more motile and phagocytic, and
106 efficiently induce T cell proliferation.
107
108

Results

Myeloid cells specifically accumulate at the maternal-fetal interface

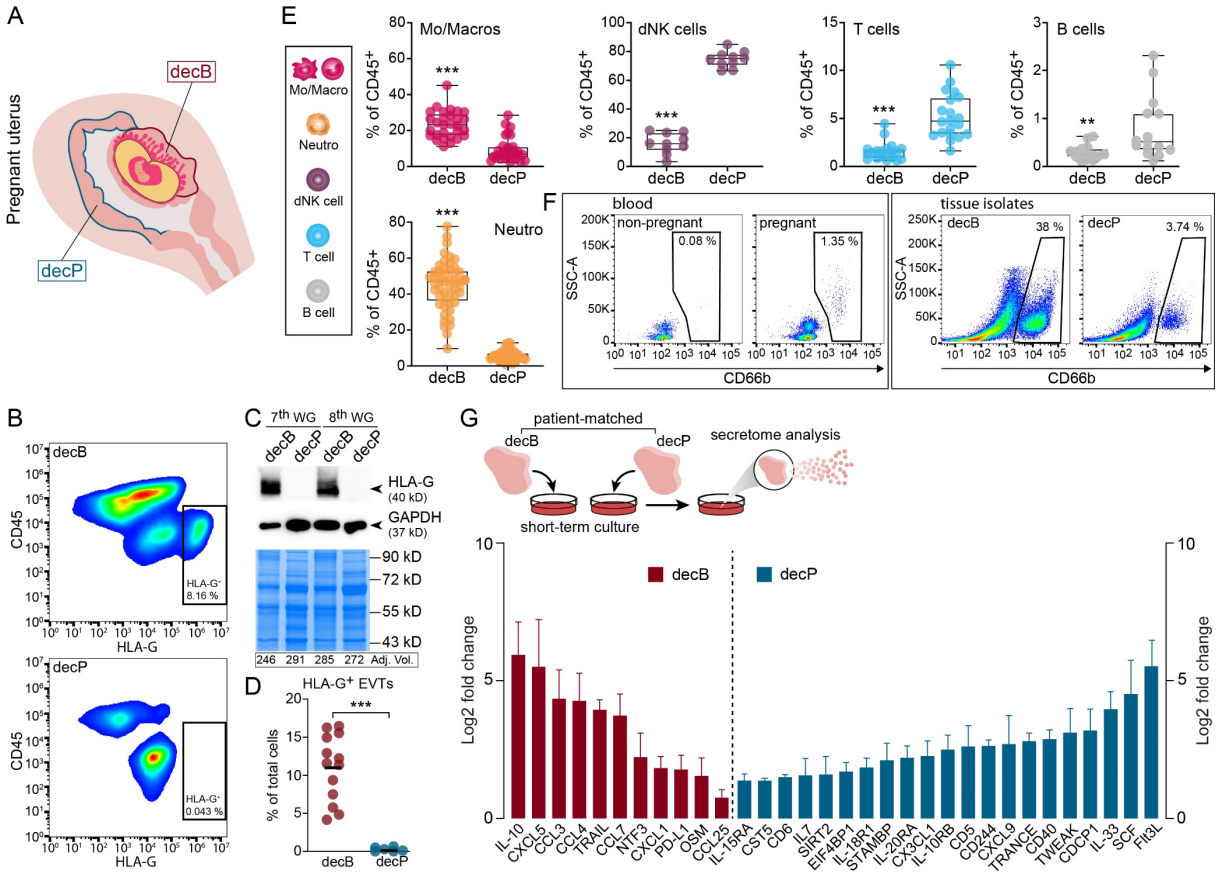

Figure 1.**Investigation of immune cell distributions in first-trimester decidual samples identifies myeloid cell accumulation in first-trimester decB tissues. (A)** Schematic drawing of a human pregnant uterus during the first trimester of pregnancy indicating decidua basalis (encircled by a red line, decB) and decidua parietalis (encircled by a blue line, decP). **(B)** Representative flow cytometry plots of decB and decP tissue cell isolates demonstrating distribution of CD45$^+$ immune cells and HLA-G$^+$ EVTs. The percentages of HLA-G$^+$ EVTs are indicated. **(C)** A representative western blot of two sets of donor-matched decB and decP protein lysates probed with antibodies against HLA-G is shown. The expression of GAPDH was determined to control for successful protein transfer and immunodetection. A stain-free system guaranteed equal total protein loading prior to blotting. Adjusted volumes (Adj. Vol.) of total band intensities are indicated underneath the stain-free gel images. **(D)** Quantification of HLA-G$^+$ EVTs in first-trimester decB (n = 14) and decP (n = 7) cell isolates, analyzed by Student's t-test. The center line represents the mean. **(E)** Bar graphs show the percentages of Mo/Macros (n = 31 pairs), dNK cells (n = 13 pairs), T cells (n = 21 pairs), B cells (n = 16 pairs) and Neutros (n = 53 pairs) of the total CD45$^+$ leukocyte population in donor-matched decB and decP tissue isolates. **(F)** Representative flow cytometry plots of isolated PBMCs from the blood of healthy non-pregnant and pregnant female donors (left panel) and donor-matched decB and decP tissue isolates (right panel). The gates represent the frequency of low-density CD66b$^+$ neutrophils of the CD45$^+$ PBMC fraction obtained by LymphoPrep®. **(G)** Summary data (log2 fold change, n = 4) for the significant differences in secreted factors from patient-matched decB and decP tissue explants after 20 h in culture measured by the proximity extension assay (www.Olink.com). The schematic drawing shown on the top illustrates the experimental set-up. Data are represented as mean + SD (standard deviation). Significances were calculated using multiple t-tests. **, P ≤ 0.01. decGE, decidual glandular epithelium; EVT, extravillous trophoblast; Mo/Macro, monocytes, macrophages; Neutro, neutrophils; dNK cell, decidual natural killer cell; WG, week of gestation.

In this study, we aimed at identifying placentation-specific immune modulation in the human decidua during early human pregnancy. To this end, we established a cohort of first-trimester decidual samples including areas affected by placentation (decidua basalis, decB) and donor-

137 matched areas that do not interact with villous placental tissues (decidua parietalis, decP) (Fig.
138 1A). The absence or presence of HLA-G, a marker for EVTs, served as an additional indicator
139 to distinguish decP from decB (Fig. 1, B and C), respectively. An overview of our tissue
140 sampling strategy is outlined in Fig. S1, A and B. First, decB and decP samples were
141 morphologically identified based on well-described characteristics (Loke, 1996). Decidua
142 parietalis tissue has a visible smooth mucosal covering (Fig. S1 B), shows the presence of
143 glands and luminal epithelium (Fig. S1 C) as well as a significantly higher cellular density when
144 compared to matched decB samples (Fig. S1 D). In contrast, we identified decB by its
145 hemorrhagic appearance and the presence of numerous EVTs invading the stroma and
146 vasculature (Fig. S1 B and Fig. S1 E). Overall, we found that cell isolates from first-trimester
147 decB tissues contain on average 11 % (± 4.34 % S.D.) of HLA-G^{+} EVTs compared with < 0.05
148 % of EVTs in decP tissues (Fig. 1 D) and that the total cellular density is significantly lower in
149 decB when compared to matched decP samples (Fig. S1 C). Next, we defined the distribution
150 of the major immune cell subtypes in decB and decP tissues, revealing an accumulation of
151 myeloid CD45^{+}CD14^{+} monocytes/macrophages and CD45^{+}CD66b^{+} neutrophils in decB
152 samples (Fig. 1 E). A representative flow cytometry gating strategy is shown Fig. S2 A and B.
153 We also considered contaminating blood a possible reason for the decB-specific neutrophil
154 accumulation. To this end, we examined decB tissues by H&E and IF stainings against CD66b
155 and confirmed the presence of interstitial neutrophils (Fig. S1 E). Ficoll® gradient centrifugation
156 revealed a significantly higher CD66b^{+} low-density neutrophil population in decB (mean =
157 41.48 %, ± 14.57 % S.D., n = 4) when compared to decP (mean = 3.37 %, ± 1.08 % S.D., n =
158 4) or blood samples from pregnant (mean = 1.29 %, ± 0. 19 % S.D., n = 3) and non-pregnant
159 women (mean = 0.18 %, ± 0.13 % S.D., n = 3) (Fig 1 F). Moreover, while decB-derived CD66b^{+}
160 neutrophils show a typical CD14^{-}, HLA-DR^{-}, CD15^{dim}, CD11c^{dim}, CD33^{dim}, CD11b^{+} and CD16^{+}
161 expression pattern, they lack the blood neutrophil marker CD62L (L-selectin) (Fig. S1 F). As
162 our focus in this study was on decidual macrophages, we re-calculated our established
163 immune cell distribution by excluding CD66b+ neutrophils, resulting in a significantly higher
164 proportion of macrophages in decB tissue isolates (Fig. S1 G). Well in line, comparative

165 analyses of secreted factors from decB and decP tissue explants revealed an overrepresented
166 myeloid-associated cytokine signature in decB tissues, including IL-10, CXCL1, CCL3, CCL4,
167 CXCL5, and suppressors of T cell responses (TRAIL and PD-L1). In contrast, decP samples
168 showed elevated levels of factors involved in T cell, DC, and NK cell immunity such as IL-7,
169 CXCL1, sCD5, sCD6, TRANCE or Flt3 (Fig. 1 G).

170

171 **Formation of decB is associated with the accumulation of tissue-resident macrophages**

172 To further increase the resolution of our data we applied specific markers to dissect
173 macrophages from infiltrating blood monocytes. *In situ* double and triple immunofluorescence
174 (IF) staining confirmed that all $CD14^+$ cells residing in the decB and decP are positive for the
175 pan macrophage marker CD68 and double-positive for CD163 and CD206 (Fig. S3 A - C).
176 Subsequent flow cytometry analysis of decidual cell isolates revealed two $CD14^+$ populations,
177 one lacking CD163 and CD206 expression and the other highly positive for both tissue
178 macrophage markers (Fig. 2 A). While the latter $CD163^+CD206^+$ population showed a typical
179 enlarged cell size and morphology with abundant vacuoles as well as high autofluorescence,
180 as is commonly observed in macrophages (McGovern et al., 2014), $CD14^+CD163^-CD206^-$ cells
181 displayed a morphology typical for monocytes such as smaller cell size or little granularity (Fig.
182 2, B and C). Bulk RNA-seq confirmed this notion by demonstrating that $CD14^+CD163^+CD206^+$
183 cells express typical hallmark genes of tissue-resident macrophages such as *MERTK*, *CD68*,
184 *MAFB* or *FCGR2A* (Xue et al., 2014) and express comparatively low levels of monocyte marker
185 genes including L-selectin (*SELL*), *S100A12*, *S100A8*, and *S100A9* (Fig. 2 D and Fig. S3 D).
186 Indeed, IF-analysis shows that $CD14^+S100A12^+$ monocytes are found in the lumen of decidual
187 vessels and not in the tissue stroma (Fig. S3 E).

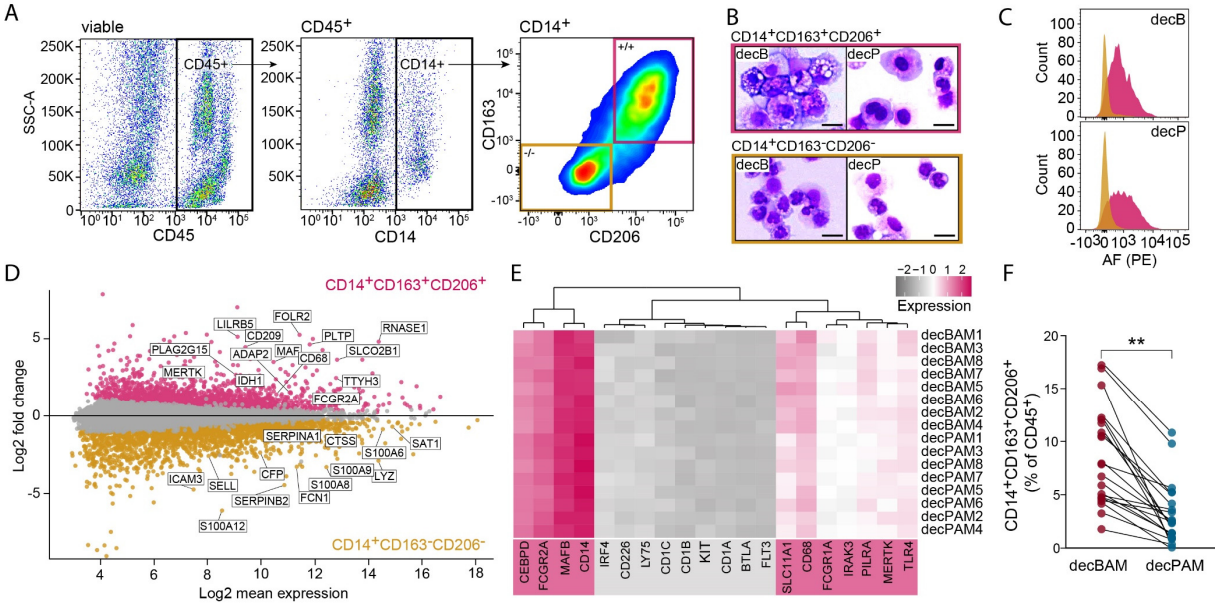

Figure 2. **Isolation and characterization of tissue-resident decidual macrophages (A)** Flow cytometry gating strategy used to identify tissue-resident decidual macrophages by a CD45$^+$CD14$^+$CD163$^+$CD206$^+$ expression profile. Pink gate, CD14$^+$CD163$^+$CD206$^+$ macrophages. Orange gate, CD14$^+$CD163$^-$CD206$^-$ monocytes. **(B)** Macrophage (pink rectangle) and monocytic (orange rectangle) populations from decB and decP were sorted and stained by Giemsa staining. Representative images of *n* = 4 experiments. Scale bar, 20 µm. **(C)** Representative flow cytometry plots identifying autofluorescence (AF) in isolated CD14$^+$CD163$^+$CD206$^+$ (pink histogram) and CD14$^+$CD163$^-$CD206$^-$ (orange histogram) cell isolates from decB and decP. **(D)** MA plot of differentially expressed genes (DEGs) from RNA-seq. Pink and orange dots represent significantly up- or down-regulated DEGs in isolated CD14$^+$CD163$^+$CD206$^+$ (n = 8 pairs) and CD14$^+$CD163$^-$CD206$^-$ (n = 4 pairs) cells from decB and decP tissues. **(E)** Heatmap showing expression of macrophage (underlaid with pink)- and DC (underlaid with grey)-associated hallmark genes in isolated decBAM and decPAM. **(F)** Dotplot demonstrating distribution of CD14$^+$CD163$^+$CD206$^+$ decBAMs and decPAMs in patient-matched first-trimester decB and decP samples (n = 21 pairs). Patient-matched samples are indicated via connected dot plots. P-value was generated using paired t-test. **, P ≤ 0.01. decB, decidua basalis; decP, decidua parietalis; decBAM, decB-associated macrophage; decPAM, decP-associated macrophage.

Next, we analyzed whether our isolated decidual macrophage populations may express DC core markers retrieved from various hallmark papers deciphering macrophage and DC signature gene expression in human and mice (Gautier et al., 2012; McGovern *et al.*, 2014; Tamoutounour et al., 2013). As expected, decidual macrophages express conserved lineage markers such as *MERTK* and *MAFB* as well as other typical markers for human and mouse macrophages, including *CD14*, *CD68*, *CEBPD*, *FCGR1A* (CD64) or *FCGR2A* (CD32). In contrast, DC-associated lineage markers such as *CD1A*/*B*/*C*, *CD226*, *FLT3* or *KIT* were absent from both populations (Fig. 2 E). By considering our established markers for tissue-residency we were able to show a decB-associated accumulation of tissue macrophages (Fig. 2 F). Finally, we termed macrophages obtained from different decidual compartments decBAMs and decPAMs, respectively. These data show that placentation is associated with increased numbers of true tissue-resident macrophages.

217 **Accumulation of decidual tissue macrophages is associated with *in situ* proliferation**

218 We next sought to determine the potential of decB to recruit neutrophils and macrophages.
219 Therefore, we generated conditioned media (CM) from cultivated patient-matched decB and
220 decP tissue samples and performed chemoattractant assays using isolated PBMCs or
221 neutrophils from peripheral blood samples. These assays revealed no differential effect
222 between decB- and decP-CM in the recruitment of $CD14^+$ blood-derived monocytes (Fig. 3 A)
223 or other PBMCs, including T cell subtypes, B cells or NK cells (Fig. 3 A, Fig. S4 A). In contrast,
224 separate assays showed that decB-CM exert a significantly higher potential to attract blood
225 neutrophils (Fig. 3 B). Well in line, culture media of decB tissues contained high levels of well-
226 described neutrophil chemoattractants including CXCL1, CXCL8, S100A8, and S100A9
227 (Kolaczkowska and Kubes, 2013; Zenz et al., 2005) (Fig. 3 C). Strikingly, *in situ* IF staining
228 showed significantly more $CD14^+Ki67^+$ macrophages in decB tissues when compared with
229 decP sections (Fig. 3 D). Decidual tissue macrophages also expressed a wide array of cell
230 cycle markers including CCNA1, pRB, and CDK1 (Fig. 3 E). In addition, we observed the
231 presence of mitotic figures in tissue-resident $CD14^+$ decidual macrophages (Fig. 3 E). Flow
232 cytometry-sorted decB macrophages Finally, an *ex vivo* proliferation assay determining EdU
233 incorporation into cultivated decidual explants revealed that decBAMs are capable of *de novo*
234 DNA synthesis, again to a greater extent than decPAMs (Fig. 3 F). Representative low
235 magnification pictures showing $CD14^+$ $ki67^+$, $CD14^+CCNA1^+$, $CD14^+$ $CDK1^+$, $CD14^+pRB^+$, and
236 $CD14^+$ EdU^+ decBAMs are represented in Fig. S4 B - D.

237

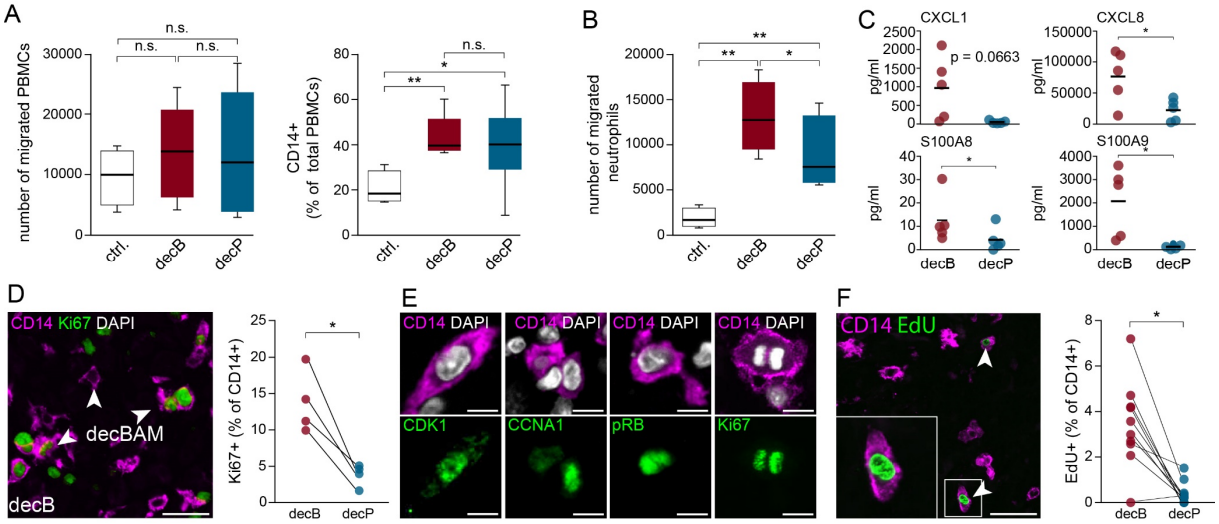

Figure 3. **decB-associated accumulation of myeloid cells is accomplished by chemoattractant factors and local proliferation of decBAMs (A)** Migratory response of PBMCs (left diagram) and CD14⁺ blood cells (right diagram) to culture medium containing decB- or decP-CM (1:4, n = 8). Decidua culture medium was used as a control. P-values were generated using Repeated-measures ANOVA with Tukey's multiple comparison test. **(B)** Migratory response of blood neutrophils to culture medium without or with decB- and decP-CM (1:2, n = 4). Boxes in box plots represent upper and lower quartiles. The center line represents the median. Whiskers show the minimum and maximum of the data. P-values were generated using Repeated-measures ANOVA with Tukey's multiple comparison test. **(C)** Secretory profile of cultivated (20 hours), patient-matched decB and decP explants (n = 5 pairs) measured by bead-based multiplex immunoassays. Dots show measured levels in pg/ml. The center line represents the mean. P-values were generated using paired t-tests. **(D)** Representative IF staining of a first-trimester decB tissue section showing CD14 (magenta) and Ki67 co-staining (green). Quantification of four patient-matched decB and decP tissue samples is shown to the right by a dot plot. Each dot represents the percentage of Ki67⁺CD14⁺ double-positive cells for each tissue sample (n = 4 pairs). Scale bar, 20 µm. Patient-matched samples are shown in connected dot plots. P-value was generated using a paired t-test. **(E)** IF co-staining of first-trimester decB tissue sections showing cell cycle markers including CDK1, CCNA1, pRB in green and CD14 in magenta. The two images to the right upper and lower panel demonstrate a Ki67 expressing mitotic figure in a CD14⁺ cell. DAPI (white) was used to visualize nuclei. Scale bars, 2 µm. **(F)** Representative IF staining of a cultivated decB explant tissue demonstrating EdU (green) incorporation into CD14⁺ (magenta) macrophages, indicated by arrowheads. Inset picture shows a EdU+ macrophage at higher magnification. Quantification of EdU incorporation into CD14⁺ macrophages of cultivated decB and decP first-trimester tissue explants. Each dot represents the percentage of CD14⁺ EdU⁺ cells for each tissue sample evaluated (n = 10 pairs). Patient-matched samples are indicated via connected dot plots. Scale bar, 20 µm. P-value was generated using a paired t-test. *, P ≤ 0.05; **, P ≤ 0.01, n.s.: not significant. decB, decidua basalis; decP, decidua parietalis.

These results suggest that decB-specific accumulation of tissue macrophages is driven by *in situ* proliferation and that, as expected, neutrophils are specifically recruited from blood.

decBAMs show a distinctive transcriptional and secretory phenotype

In-depth analysis of our bulk RNA-seq-based transcriptome data revealed substantial differences between isolated patient-matched decBAMs and decPAMs, which are shown to form two distinct groups by principal component analysis (PCA) (Fig. S5 A). We identified 1127 significantly differentially expressed genes (DEGs, adjusted p value < 0.05) between decBAMs (512 up) and decPAMs (615 up) (Fig. 4 A). Immune-related DEGs included *ITGAX* (CD11c), *CD44*, *CXCL2*, and *ANPEP* in decBAMs, and *AXL*, *GAS6*, *SELENOP*, *C3*, and *IL2RA* in

273 decPAMs (Fig. 4 A). IF- and flow cytometry-based analyses confirmed higher expression of
274 HMOX1, CD44, and CD11c protein in decBAMs (Fig. 4 B). Single channels and lower
275 magnification pictures of CD44 and HMOX1 stainings are shown in Fig. S5 B and C. Moreover,
276 functional gene enrichment analysis revealed that gene sets involved in granulocyte/neutrophil
277 activation and myeloid immune responses were overrepresented in decBAM-associated DEGs
278 (Fig. S5 D). CD11c has already been suggested as a marker to distinguish between different
279 decidual macrophage populations, however not in the context of regionally distinct decidual
280 tissues (Houser *et al.*, 2011). DEGs highly expressed in CD11c^{hi} macrophages identified by
281 Houser et al. mainly coincide with decBAM upregulated genes, and conversely, CD11c^{lo}
282 associated transcripts show a clear overlap with decPAM-associated gene signatures (Fig. S5
283 E). Prior to our study, three tissue-resident myeloid cell types have been identified by single-
284 cell (sc) RNA-seq, designated as decidual macrophage 1 (dM1), decidual macrophage 2 (dM2)
285 and dendritic cell 1 (DC1) (Vento-Tormo *et al.*, 2018). A third decidual macrophage subtype
286 (dM3) identified in this study, later defined as a subtype of placenta-associated maternal
287 macrophages (PAMMs), does not constitute a decidua-resident cell type but is found in the
288 intervillous blood space, adhering to placental villi (Thomas *et al.*, 2021). Our comparative
289 computational approach showed that transcripts upregulated in decPAMs clearly associated
290 with the dM2 phenotype whereas decBAMs showed a strong overlap with the previously
291 identified dM1-associated genes both in global and single gene expression pattern (Fig. 4 D).
292 Well in line, decBAM- or decPAM-associated DEGs identified by our bulk RNA-seq analysis
293 were also differentially regulated in dM1 and dM2 populations (Fig. 4 E). In addition, decBAMs
294 showed a closer similarity with dM3-specific signatures, compared to decPAM (Fig. S5 F). To
295 this end, we isolated PAMMs and confirmed their transcriptional overlap with dM3 signatures
296 but also with maternal blood-derived immune cells such as monocytes or dendritic cells (DC2)
297 (Fig. S 5 F). Overall, these data confirm that PAMMs likely originate from blood monocytes
298 (Thomas *et al.*, 2021). Next, we digested decB and decP tissues in order to study the
299 secretome of isolated and short-term cultivated EVTs, neutrophils, decBAMs, and decPAMs
300 (Fig. 4 F). All cells were sorted by FACS except for EVTs, which were isolated via magnetic

beads conjugated with anti-HLA-G. Due to their large size, EVTs are very sensitive to the high pressure and shear forces in a cell sorter and show improved viability when sorted over magnetic columns. Viability and purity of EVTs were confirmed by flow cytometry after isolation (Fig. S5 G).

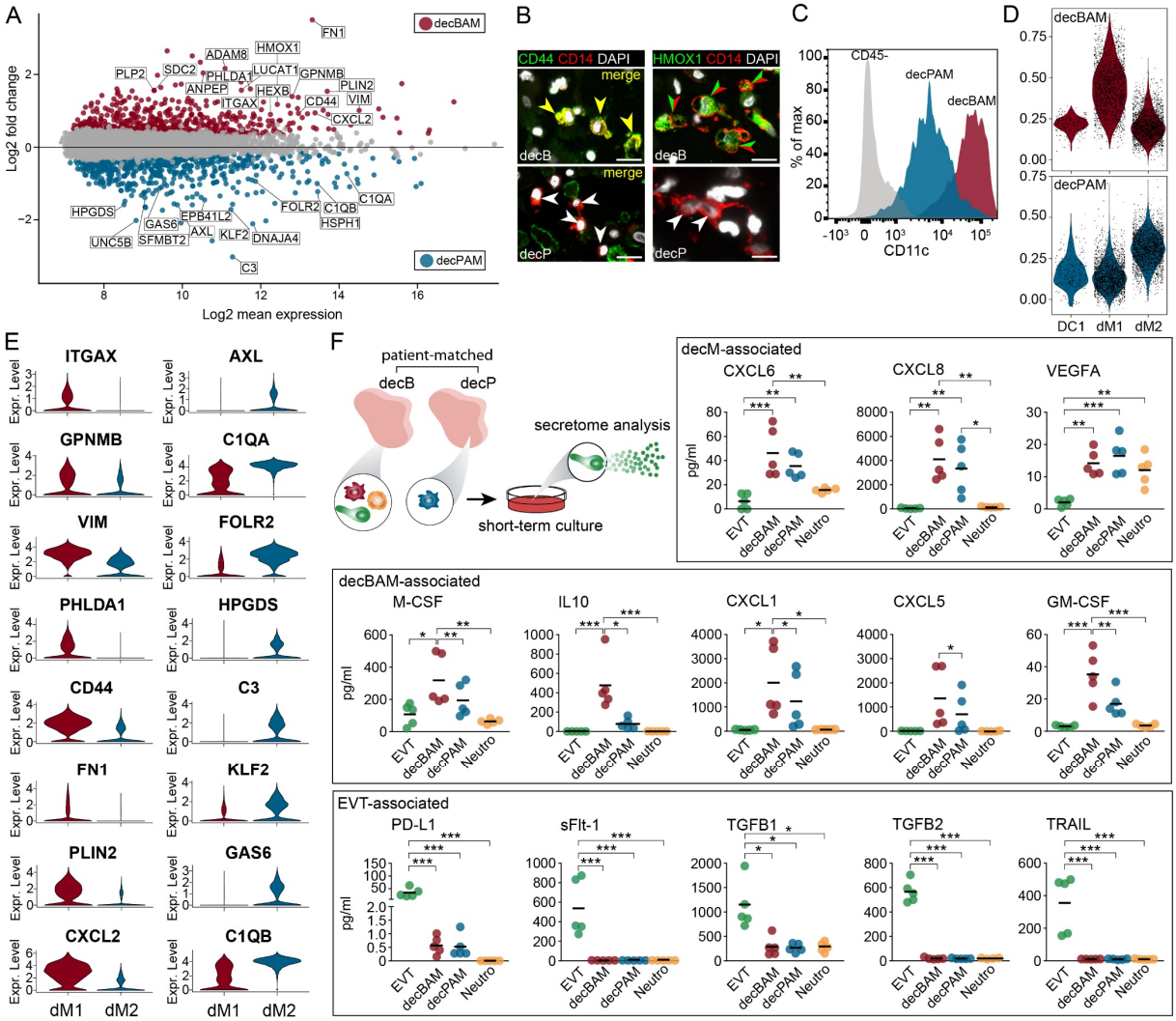

Figure 4. **First-trimester decBAMs and decPAMs differ in their transcriptional and secretory profile (A)** MA plot of DEGs from RNA-seq. Red and blue dots represent significantly up- or down-regulated DEGs in patient-matched isolated $CD14^{+}CD163^{+}CD206^{+}$ decBAMs and decPAMs (n = 8 pairs). **(B)** Representative IF co-staining of a first-trimester paraffin-embedded decB and decP tissue section showing HMOX1 and CD44 expression (green) in $CD14^{+}$ tissue macrophages (red). Arrowheads in yellow (left) or in green and red (right) indicate double positive cells. Scale bars, 20 µm. **(C)** Representative flow cytometric analysis of isolated decBAMs and decPAMs showing CD11c expression. **(D)** Violin plots showing expression of decBAMs (red) and decPAMs (blue) signatures in selected scRNA-seq clusters (Vento-Tormo et al., 2018). **(E)** Violin plots presenting expression of selected decBAM- and decPAM-associated gene transcripts in dM1 and dM2 scRNA-seq clusters (Vento-Tormo et al., 2018). **(F)** Secretory profile of magnetically sorted and cultivated (20 h) EVTs, decBAMs, decPAMS and neutrophils, determined by bead-based multiplex immunoassays (n = 5 pairs). Measured levels (pg/ml) of growth factors, chemokines and cytokines are shown as dots and the group mean is shown as centered line. The schematic drawing shown on the top illustrates the experimental set-up. P-values were generated using One-way ANOVA with Tukey's multiple comparison test. *, $P \leq 0.05$; **, $P \leq 0.01$; ***, $P \leq 0.001$. decB, decidua basalis; decP, decidua parietalis; decM, decidual macrophage; decBAM, decB-associated macrophage; decPAM, decP-associated macrophage; EVT, extravillous trophoblast; Neutro, neutrophil.

323 We determined secretion of cytokines and growth factors, which were selected based on our
324 previous analyses and their involvement in myeloid or neutrophil immunity and function. In
325 parallel, we measured these factors in decB and decP tissue explant CMs to control for a
326 possible loss of tissue specificity upon single cell culture (Fig. S6 A). While decBAMs culture
327 media contained significantly higher levels of CXCL1, CXCL5, GM-CSF, M-CSF, and IL-10,
328 decBAMs and decPAMs were equally efficient in releasing CXCL6, as well as high levels of
329 CXCL8. Among the macrophage-associated factors, the measured GM-CSF levels were the
330 lowest. All three immune cell populations secreted low but significantly induced levels of
331 VEGFA, when compared to EVTs. Our analyses further revealed that EVTs are efficient
332 producers of sPD-L1, TGFβ1, TGFβ2 and TRAIL. As a control for cell identity and
333 differentiation, we additionally analyzed EVT-specific sFlt-1 (Fan et al., 2014) (Fig. 4 F). Well
334 in line, EVT-, neutrophil-, and decBAM-associated factors were also significantly enriched in
335 decB-CM with the exception of M-CSF, GM-CSF and CXCL1, the latter showing elevated but
336 not significantly increased values (Fig. S6 A). Lastly, neutrophils secreted significantly higher
337 amounts of S100A8, S100A9, and MMP9 (Fig. S6 B).
338 In summary, decBAMs differ substantially from decPAMs by a specific transcriptome and
339 secretome.
340

341 **decBAMs induce Tregs and are suppressed in their APC-like function**

342 Our IF analyses show a strong difference in decBAM and decPAM appearance, the latter
343 exhibiting a more dendritic cell-like morphology (Fig. 5 A). Higher magnification clearly shows
344 an enhanced spindle-shaped morphology and formation of pseudopodia in decPAMs, implying
345 a more motile phenotype (Fig. 5 A). Interestingly, CD11c^{lo} decPAMs also showed a more
346 prominent staining with antibody against HLA class II molecules (Fig. 5 B). Single channel and
347 lower magnification pictures of CD14/CD11c and CD14/HLA-DRA co-stainings are shown in
348 Fig. S7 A and B. Well in line, flow cytometry analysis reveals suppressed HLA-DR cell surface
349 expression in decBAM cell isolates, which express high levels of CD11c (Fig. 5C). In contrast,
350 decPAMs show high expression of HLA-DR and induced transcript levels of *HLA-DOA*, *HLA-*

DPA1 as well as *HLA-DRB1* and tended to show higher but not significantly elevated levels of *HLA-DRA* (Fig. S7 C). To test whether decPAMs indeed show pronounced APC-like functions we isolated decBAMs and decPAMs from the same donors and performed functional *in vitro* assays. Comparative video-based analysis of freshly isolated decidual macrophages indeed showed that decPAMs (Video 1) moved significantly faster than decBAMs (Video 2) when tracked in real time (Fig. 5, D and E). In addition, decPAMs also showed a significantly higher phagocytic activity when compared to decBAMs (Fig. 5, F and G). A recent study suggests that decidual macrophages are efficient inducers of Treg formation (Salvany-Celades et al., 2019).

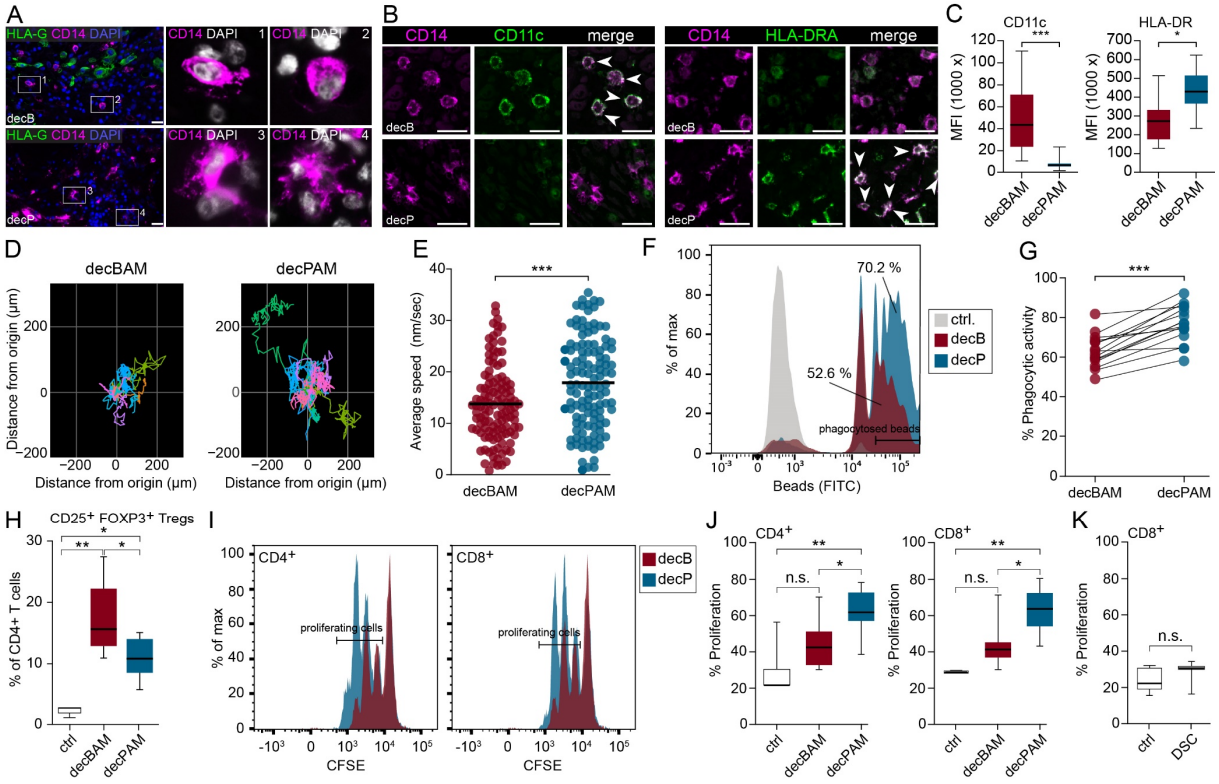

Figure 5. **decBAMs show a pregnancy-tolerating phenotype by suppressed APC-like function and enhanced ability to induce Treg formation. (A)** Representative IF staining of decB and decP tissue sections with antibodies against HLA-G (green) and CD14 (magenta). Zoomed insets on the right show appearance of CD14$^+$ macrophages in areas invaded by HLA-G$^+$ EVTs (1, 2) and those unaffected by placentation (3, 4). Representative images of *n* = 25 experiments. Scale bar, 20 µm. **(B)** IF co-stainings of first-trimester paraffin-embedded decB and decP tissue sections showing CD11c (green, left panel), HLA-DRA (green, right panel) and CD14 (magenta). White arrowheads indicate double positive cells. Representative images of *n* = 4 experiments. Scale bar, 50 µm **(C)** Median fluorescence intensity (MFI) of CD11c (n = 29 pairs= and HLA-DR (n = 8 pairs) was determined by flow cytometry in CD45$^+$CD14$^+$CD163$^+$CD206$^+$ decBAMs and decPAMs (n = 8 pairs) as indicated. The center line represents the median. Whiskers show the minimum and maximum of the data. P-values were calculated using paired Student´s t-test. **(D)** Representative cell tracks of isolated and short-term (24 h) cultivated decBAMs and decPAMs were generated by live-cell microscopy (capture rate = 12 frames/h). Cell tracks were color-coded for each monitored cell over 12 h. **(E)** Dots present average speed of captured individual cell tracks (n = 117) of decBAMs and decPAMs cultures (n = 8 pairs). 7 outliers were removed by Grubbs' test. The center line represents the mean. P-value was generated using Student's t-test. **(F)** Representative flow cytometric analysis of phagocytosed FITC-labeled beads by decBAMs and decPAMs after 2 h of incubation. **(G)** Dots represent the percentage of phagocytosed FITC-labeled beads of each individual experiment performed (n = 15 pairs). Patient-matched samples are indicated via connected

379 dot plots. P-value was generated using a paired t-test. **(H)** Box plots show the potential of decBAMs and decPAMs
380 to induce $CD4^+FOXP3^+CD25^+$ Tregs from isolated $CD3^+$ blood T cells (n = 5). P-value was generated using paired
381 t-test. **(I)** Representative flow cytometry plots showing CFSE dilution in $CD4^+$ and $CD8^+$ isolated blood T cells
382 stimulated with anti-CD3/CD28 in the presence of decBAMs (red histogram) or decPAMs (blue histogram). **(J)** Box
383 plots represent the median level of the percentage of dividing $CD4^+$ and $CD8^+$ T cells (at least one cell division as
384 defined by CSFE dilution) in the absence or presence of decBAMs and decPAMs (n = 8). Box plots represent
385 median values ± SEM. Boxes in box plots represent upper and lower quartiles. The center line represents the
386 median. Whiskers show the minimum and maximum of the data. DAPI was used to visualize nuclei. P-values were
387 generated using one-way ANOVA with Tukey's multiple comparison test. *, $P \leq 0.05$; **, $P \leq 0.01$; ***, $P \leq 0.001$.
388 **(K)** Box plots show the median levels of dividing $CD8^+$ T cells in the absence or presence of DSCs (n = 3). P-values
389 were calculated using Student´s t-test. decB, decidua basalis; decP, decidua parietalis; decBAM, decB-associated
390 macrophages; decPAM, decP-associated macrophages; MFI, median fluorescence intensity; Tregs, regulatory T
391 cells.
392
393 By studying this phenomenon, we found that induction of $CD4^+CD25^+FOXP3^+$ Tregs is not a
394 uniform feature of decidual macrophages since Treg induction was in particular executed by
395 decBAMs (Fig. 5 H). To further test for dendritic cell-like function, we studied the potential of
396 decidual macrophages to activate blood-derived T cells. To this end, we cultivated T cells from
397 healthy donors with decBAMs or decPAMs in a ratio of 10:1. In line with our previous results,
398 mainly decPAMs are able to trigger proliferation in both $CD4^+$ helper T cells and $CD8^+$ cytotoxic
399 T cells (Fig. 5, I and J). We observed no induction of $CD8^+$ T cells when blood-derived T cells
400 were incubated with decidual stroma cells (DSCs), confirming that our assay is not disturbed
401 by reactivity against allogeneic HLA class I molecules (Fig. 5 K).
402 Altogether, we show that decBAM are impaired in their ability to migrate, phagocytose, and
403 promote T cell proliferation but are efficient inducers of Tregs.
404
405 **The secretome of EVTs induces a decBAM-like phenotype**
406 Since our secretome screen of isolated EVTs revealed high secretion of immunomodulatory
407 factors (Fig. 4 F) we assumed that EVTs can alter decidual macrophage activation and
408 function. In order to avoid preconditioning by a decB environment likely under the control of
409 EVTs, we decided to test this by studying EVT-dependent effects on either whole decP tissue
410 explants or isolated decPAMs. To this end, we treated isolated decP tissue explants with EVT-
411 conditioned media (EVT-CM) and investigated possible alterations in decPAMs upon treatment
412 (Fig. 6 A). Immunofluorescence-based analysis indeed showed that addition of EVT-CM
413 significantly increases CD44 expression of decPAMs *in situ* to a comparable level as detected
414 in decB tissue explants (Fig. 6 B). Next, we exposed isolated decPAMs to 50% EVT-CM and

found a significantly reduced motility and phagocytic activity (Fig. 6, C and D). EVTs secrete high levels of the immunomodulatory factors TGFβ1 and TGFβ2, well studied for their pleiotropic effects on macrophages, as well as high levels of PD-L1, which has recently been suggested to inhibit macrophage phagocytosis when expressed by tumor cells (Gordon et al., 2017). However, the suppressive activity of EVT-CM towards the phagocytic activity of decPAMs was not reversed by the addition of any of the blocking antibodies against TGFβ or PD-L1 (Fig. 6 E). Next, we investigated the effect of EVT-CM on the ability of decPAMs to interfere with T cell function. While neither EVT-CM alone nor in combination with decPAMs affected Treg differentiation (Fig. 6 F), we found a significantly reduced decPAM-dependent activation of $CD4^+$ and $CD8^+$ T cells upon treatment with EVT-CM (Fig. 6 G).

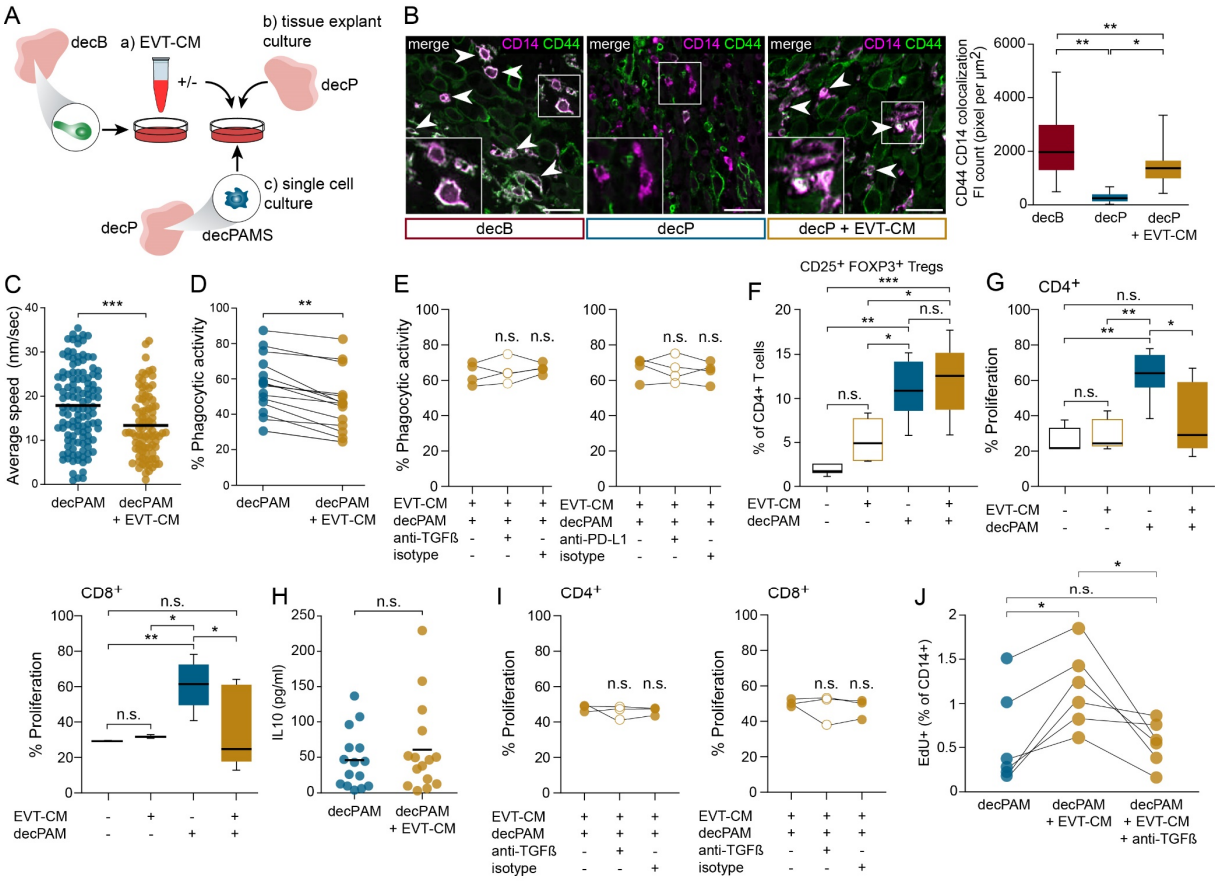

Figure 6. **decPAMs are functionally reprogrammed by the secretome of EVTs (A)** Schematic drawing to illustrate the experimental set up. EVTs were isolated by magnetic beads conjugated with anti-HLA-G and cultivated for 20 h to generate EVT-CM (a) used to stimulate decP tissue explants (b) or FACS-isolated decPAMs (c). **(B)** Representative double IF stainings using antibodies against CD14 (magenta) and CD44 (green) investigating overlapping CD14 CD44 expression in unstimulated decB and decP tissue cultures and EVT-CM stimulated decP explant cultures. Examples of overlapping signals are marked by white arrow heads. Box plots indicate median value of white pixels per μm^2 (generated by overlays of green and magenta colored CD14/CD44 co-stainings). P-values were generated using one-way ANOVA with Tukey's multiple comparison test. Scale bars, 20 µm **(C)** Diagram shows average speed of each cell tracked (n = 90) in independent experiments using isolated decPAMs either without or with stimulation with 50% EVT-CM (n = 6 pairs). 7 outliers were removed by Grubbs' test. The center line represents the mean. P-values was generated using a paired t-test. **(D)** Dot plot represents the

437 percentage of phagocytosed FITC-labeled beads of each individual experiment performed (n = 14 pairs). Patient-
438 matched samples are indicated via connected dot plots. P-value was generated using a paired t-test. **(E)**
439 Phagocytosis assays were performed in the presence of EVT-CM alone, with isotype control or blocking antibodies
440 for TGFβ or PD-L1. **(F)** Box plots show the potential of decPAMs and/or EVT-CM to induce CD4+FOXP3+CD25+
441 Tregs (n = 5). Box plots represent median values ± SEM. Boxes in box plots represent upper and lower quartiles.
442 The center line represents the median. Whiskers show the minimum and maximum of the data. P-values were
443 generated using One-way ANOVA with Tukey's multiple comparison test. *, P ≤ 0.05; **, P ≤ 0.01, n.s.: not
444 significant. **(G)** Box plots show the percentage of proliferative $CD4^+$ or $CD8^+$ T cells stimulated with anti-CD3/CD28
445 in the absence or presence of decPAMs and/or EVT-CM (n = 7). P-values were generated using one-way ANOVA
446 with Tukey's multiple comparison test. **(H)** Potential of short-term (20 h) cultivated decPAMs to secrete IL-10 (pg/ml)
447 stimulated without or with EVT-CM (n = 15 pairs). **(I)** Box plots represent the percentage of dividing $CD4^+$ and $CD8^+$
448 T cells (at least one cell division as defined by CSFE dilution) stimulated with decPAMs and EVT-CM in the absence
449 or presence of isotype control or a blocking antibody for TGFβ (n = 3). P-values were generated using one-way
450 ANOVA with Tukey's multiple comparison test. **(J)** Percentage of EdU^+ nuclei in $CD14^+$ macrophages of cultivated
451 decP first-trimester tissue explants. Each dot represents the percentage for each tissue sample evaluated (n = 6
452 pairs). Patient-matched samples are indicated via connected dot plots. P-values were generated using Repeated-
453 measures ANOVA with Tukey's multiple comparison test. Boxes in box plots represent upper and lower quartiles.
454 The center line represents the median. Whiskers show the minimum and maximum of the data. *, P ≤ 0.05; **, P ≤
455 0.01; ***, P ≤ 0.001, n.s.: not significant. decB, decidua basalis; decP, decidua parietalis; decBAM, decB-associated
456 macrophages; decPAM, decP-associated macrophages; EVT-CM, extravillous trophoblast-conditioned medium;
457 Tregs, regulatory T cells.
458
459
460 Given that EVT-CM alone did not suppress $CD4^+$ or $CD8^+$ T cell proliferation (Fig. 6 G) we
461 assumed an indirect effect for instance by EVT-CM-driven induction of IL-10, as previously
462 shown for cancer-derived PD-L1 (Gordon *et al.*, 2017) or by other TGFβ-driven effects on
463 decPAMs. However, EVT-CM neither altered IL-10 secretion by cultivated decPAMs nor did
464 TGFβ blockage alter the suppressive effect of EVT-CM on decPAM-induced T cell proliferation
465 (Fig. 6, H and I). Lastly, we incubated decP explant tissues with EVT-CM and found
466 significantly induced EdU incorporation into macrophages when compared to control
467 treatment. In this setting, the addition of a neutralizing antibody against TGFβ reversed the
468 growth-promoting effect of EVT-CM (Fig. 6 J).
469 In summary, these data show that EVTs have the capacity to trigger a pregnancy-tolerant
470 phenotype in macrophages via their pleiotropically acting secreted factors.
471

472 **Discussion**

473 In this study, we describe profound phenotypical and functional differences of tissue-resident
474 macrophages in dependence on their localization within the human decidua. Moreover, the
475 substantial difference between decBAMs and decPAMs in terms of transcripts, cellular
476 proteome, and secretome also translated into different functional phenotypes. Finally, we show
477 that EVT-CM is able to alter decPAMs into a phenotype functionally reminiscent of decBAMs.
478 Surprisingly, we identified a significant increase in neutrophils and macrophages at the
479 maternal-fetal interface. Except for a few studies in humans (Amsalem et al., 2014; Croxatto
480 et al., 2016) and mice (Zhao et al., 2015), decidual infiltration with neutrophils is a poorly
481 described phenomenon. To rule out incorrect tissue sampling and accidental contamination
482 with blood-derived neutrophils, we established a thorough donor-matched tissue sampling
483 strategy and, in addition, performed in-depth characterization of isolated neutrophils. In line
484 with the negative L-selectin cell surface expression pattern identified on decB-derived
485 neutrophils, we confirmed their interstitial presence using immunofluorescence and H&E
486 stainings. Pregnancy is associated with accumulating numbers of blood granulocytic myeloid-
487 derived suppressor cells (G-MDSCs) that can be distinguished from mature blood neutrophils
488 by their different densities (Bronte et al., 2016). Indeed, we confirmed a significantly increased
489 proportion of low-density neutrophils in the blood of pregnant women and found their
490 accumulation in decB cell suspensions. Further characterization of decB-derived neutrophils
491 revealed high levels of MMP-9 and the chemokines S100A8 and S100A9. While the latter two
492 have recently been suggested to serve as markers for G-MDSCs (Bronte *et al.*, 2016), MMP-
493 9 production is a feature of tumor-associated neutrophils reported to trigger tissue remodeling
494 and angiogenesis in this context (Ardi et al., 2007; Bekes et al., 2011). These data implicate
495 that decidual neutrophils exert immunosuppressive function and may have additional functions
496 in vascular remodeling.

497 We report a significant accumulation of $CD14^+$ $CD163^+$ $CD206^+$ tissue macrophages in decB
498 samples. There is a significant discrepancy in the literature regarding the frequency of
499 macrophages in the human decidua that is presumably related to the differences in techniques,

500 markers and tissues used to identify these cells (Bulmer et al., 1991; Haller et al., 1995; Helige
501 et al., 2014; Repnik et al., 2008; Solders et al., 2017). Supportive evidence for the accumulation
502 of macrophages at the maternal-fetal interface includes induced numbers of CD163^{+} cells in
503 the vicinity of invading EVTs (Helige et al., 2014), increased levels of CD206^{+} and CD209^{+}
504 cells in decB (Repnik *et al.*, 2008), elevated distribution of CD45^{+} CD14^{+} cells in decB at term
505 (Solders et al., 2017), and the accumulation of Ly6-C^{hi} monocytes/macrophages in the
506 pregnant mouse uterus (Zhao et al., 2015). To account for these disparities, we established a
507 gating strategy to identify true tissue macrophages in our optimized tissue collective. Indeed,
508 CD14^{+}CD163^{+}CD206^{+} decidual macrophages revealed high expression of lineage-associated
509 hallmark genes, typical morphology and other specific characeristics but failed to express
510 prototypical monocyte-associated markers. Similar to our results obtained by determining
511 CD14^{+} myeloid cells, we find a significant rise in CD14^{+}CD163^{+}CD206^{+} tissue macrophages
512 in decB. We further sought to explore phenotypical and functional differences between
513 decBAMs and decPAMs. Transcriptional profiling identified over 500 overexpressed DEGs in
514 decBAMs compared to decPAMs, and subsequent enrichment analysis indicated them to be
515 associated with neutrophil and myeloid cell activation. Well in line, isolated and short-term
516 cultivated decBAMs actively secrete high levels of CXCL1, CXCL5, CXCL8, IL-10, and M-CSF.
517 In particular, the latter two exert critical functions during pregnancy, for example, by inducing
518 a decidual phenotype in monocyte-derived macrophages (Lindau et al., 2021; Svensson-
519 Arvelund et al., 2015; Svensson et al., 2011) thereby acting in an autocrine self-perpetuating
520 manner. Furthermore, reduced IL-10 blood levels are associated with human pregnancy
521 disorders such as preeclampsia (Nath et al., 2020). While administration of IL-10 prevents
522 naturally occurring fetal losses (Chaouat et al., 1995), its deletion can provoke spontaneous
523 abortions in mice (Murphy et al., 2005). M-CSF has been shown to support placental function
524 by affecting EVT invasion (Hamilton et al., 1998). In addition, we find that decBAMs
525 overexpress specific cell surface markers including CD11c. While CD11c has been previously
526 proposed as a marker for different macrophage populations in the decidua (Houser *et al.*,
527 2011), our study is the first to localize CD11c^{hi} macrophages in decB. DEGs previously

528 noticed to be expressed in isolated decidual CD11c^{lo} macrophages (Houser *et al.*, 2011)
529 largely clustered into decPAM-specific transcripts and vice versa DEGs found in to be
530 expressed in CD11c^{hi} macrophages were overexpressed in decBAMs. Along these lines, our
531 comparative computational approach demonstrated that our decBAM and decPAM
532 populations share major similarities with dM1 and dM2 populations identified by scRNA-seq
533 (Vento-Tormo *et al.*, 2018), respectively. Along these lines, our study further complements
534 previous reports identifying novel decidual macrophage populations (Houser *et al.*, 2011;
535 Svensson *et al.*, 2011; Vento-Tormo *et al.*, 2018) by specifying their localization to decB and
536 decP.
537 We further revealed a significant difference in the cell surface expression of HLA class II
538 molecules in isolated decBAMs and decPAMs. Functional assays revealed that decPAMs are
539 efficient phagocytes, stimulate T cell proliferation and show a migratory phenotype. These data
540 imply that decPAMs constitute a significant tissue-resident APC population, where they serve
541 as patrolling cells to protect the maternal-fetal interface from invading pathogens. However,
542 migratory APCs are central in priming T cell responses to peripheral tissue antigens
543 (Allenspach et al., 2008; Itano et al., 2003) and thus pose a critical threat to human pregnancy
544 by potentially provoking T cell responses to placental antigens. Indeed, we find that decBAMs
545 are significantly impaired in their migratory and phagocytic activity and their potential to trigger
546 T cell proliferation. In line with this, decBAMs induced higher numbers of CD4^{+}CD25^{+}FOXP3^{+}
547 Tregs. This phenomenon is well-described for IL10- and TGFβ-secreting anti-inflammatory
548 macrophages (Ruffell and Coussens, 2015) and has also been assigned to decidual
549 macrophages (Salvany-Celades *et al.*, 2019), however not in comparison to decPAMs.
550 Accumulatively, our descriptive and functional data imply that decBAMs trigger a broad anti-
551 inflammatory environment i T cell activation and are likely one of the main inducers of
552 neutrophil influx.
553 Pioneering work in mice showed that so-called yolk sac-derived tissue-resident macrophages
554 seed into tissues during embryogenesis and are replenished by local proliferation throughout
555 life (Ginhoux and Guilliams, 2016; Palis et al., 1999). While the local renewal of tissue

556 macrophages has been confirmed in various transplantation studies in the liver (Klein et al.,
557 2007), brain (Ginhoux et al., 2010), lung (Bittmann et al., 2001; Byrne et al., 2020) and heart
558 (Bajpai et al., 2018), a definitive proof for the existence of long-lived, tissue-resident
559 macrophages in humans is missing. In our study we find that decBAMs show signs for DNA
560 synthesis in an *ex vivo* assay and a higher proliferative capacity *in situ*, compared to decPAMs.
561 Although we cannot exclude macrophage replenishment by monocyte extravasation,
562 additional *ex vivo* assays suggest that decB-CMs do not exert higher potential to attract
563 monocytes when compared to decP explant-CMs. Tissue macrophage proliferation at the
564 maternal fetal interface has further been confirmed in Hofbauer cells, which likely replenish
565 independently of the embryonic bone marrow (Thomas *et al.*, 2021). However, tissue
566 macrophage polarization greatly depends on extrinsic stimuli, regardless of ontogeny (Ginhoux
567 and Guilliams, 2016). For instance, macrophage progenitors of different origins develop into
568 fully functional alveolar macrophages (van de Laar et al., 2016) and peritoneal macrophage
569 diversity is determined by tissue-derived signals (Okabe and Medzhitov, 2014). Therefore, we
570 hypothesized that the phenotype of decBAMs depends on placenta-derived signals.
571 To test this, we incubated isolated decPAMs with CM of cultivated primary EVTs to mimic
572 trophoblast-dependent effects on decidual macrophages unaffected by placentation in utero.
573 Functional studies on viable tissue explants revealed that placenta-derived signals could
574 override the tissue-specific phenotype of decPAMs. In this setting, the addition of EVT-CM led
575 to a significant induction of proliferation and upregulation of CD44 expression, a marker of
576 decBAMs. Paralleling the phenomenon observed in decP tissue explants, EVT-CM also
577 changed the functionality of isolated decPAMs by suppressing their migratory and phagocytic
578 activity. Similar observations have been made in cancer, where tumor cells selectively inhibit
579 the phagocytosis of tumor-associated macrophages (TAMs) by avoiding the generation of
580 tumor antigen-specific cytotoxic T cells (Pathria et al., 2019). Indeed, restoration of the
581 phagocytic activity in TAMs led to cancer-specific priming of $CD8^+$ T cells (Tseng et al., 2013).
582 Similar to the reduced ability of decBAMs to trigger T cell proliferation, decPAM-mediated T
583 cell activation was also significantly suppressed upon the addition of EVT-CM. These data

584 show that EVT-derived factors play a central role in the extrinsic control of macrophage
585 function. Neutralizing antibodies targeting TGFβ, PD-L1, or IL-10 did not affect the EVT-CM-
586 dependent effects on decPAM, likely due to the pleiotropic effect of EVT-CM on decidual
587 macrophages. Indeed, another study reported that the FOXP3+ Treg-inducing effect of EVTs
588 was unaffected by the addition of neutralizing antibodies targeting CD3, HLA-C, HLA-G, ILT2,
589 TGFβ, and PD-L1 (Salvany-Celades *et al.*, 2019). The ineffectiveness of our attempts to block
590 the effect of EVT-CM likely has several reasons -one of which may be trophoblast-specific
591 glycosylation patterns. A recent report shows that specific sialylated glycans of placenta
592 antigens mediate B cell suppression (Rizzuto et al., 2022). Indeed, glycosylation alters anti-
593 body-mediated binding to PD-L1 and predicts therapy effectiveness. However, selective
594 blockage of TGFβ reversed the growth-promoting effect of EVT-CM in decPAMs. This
595 observation and our finding that isolated decBAMs secrete high levels of M-CSF imply a
596 growth-inducing autocrine loop as well as extrinsic proliferative stimuli by invasive EVTs.
597 Indeed, TGFβ1 has been shown to enhance macrophage proliferation via the induction of M-
598 CSF (Celada and Maki, 1992).
599 The generation of an immunosuppressive environment is decisive for a successful pregnancy.
600 However, our data impose that this phenomenon does not affect the entire decidua. In fact, we
601 find that macrophages further away from the placentation site, referred to as decPAM in this
602 study, show functionality of tissue-patrolling macrophages. In contrast, decBAMs residing at
603 the maternal-fetal interface exhibit significantly less pronounced APC-like function. Our study
604 further implies that this pregnancy tolerant phenotype is dictated by the placenta as EVTs can
605 be used to modify the functionality of decPAMs towards a state reminiscent of decBAMs.
606

607 **Material and Methods**

608

609 **Ethical considerations**

610 All experiments and analyses were conducted in accordance with the Declaration of Helsinki
611 as well as Austrian laws and guidelines. First trimester (6 – 10 weeks of gestation, n = 97)
612 decidual and placental tissues were derived from women undergoing elective termination of
613 pregnancy for nonmedical reasons. Pregnancy terminations were performed by surgical
614 aspiration. The use of patient material was approved by the Ethics Committee of the Medical
615 University of Vienna. Ethical approvals are annually renewed. The use of blood samples from
616 healthy control women for migration assays of PBMCs was approved by the Regional Ethics
617 Committee in Linköping, Sweden. Written informed consent was obtained from all subjects.

618

619 **Cell isolation**

620 For decidual and endometrial cell isolation, tissue was cut into small pieces using a scalpel
621 and digested using 2,5 µg/ml Collagenase IV (Worthington) and 25 mg/ml DNase I (Sigma-
622 Aldrich) with the 37°C Multi-B program of a gentleMACS Dissociator (Miltenyi Biotec). The
623 resulting single cell suspension was passed through a 70 µm cell strainer (Falcon). If
624 necessary, red blood cells were lysed by incubating cells in a buffer containing 155 mM NH4Cl,
625 10 mM KHCO3, and 0.1 mM EDTA (pH 7.3) for 5 min, before staining for flow cytometry or
626 sorting.

627 For flow cytometry and sorting, macrophages were defined as $CD45^+CD14^+CD163^+CD206^+$,
628 monocytes were defined as $CD45^+CD14^+CD163^-CD206^-$, neutrophils were defined as
629 $CD45^+CD66b^+$, and DSCs were defined as $CD45^-$ $HLA\text{-}G^-$. Dead cells were excluded using the
630 viability dye Zombie Violet (BioLegend). For generation of conditioned media, sorted cells were
631 seeded onto Nunc Cell-Culture plates (ThermoFisher) at a density of 1 million cells/ml in
632 Decidua culture medium, consisting of DMEM/F-12 without phenol red (Gibco), supplemented
633 with 10% FBS superior (Sigma Aldrich), 50 µg/ml gentamicin (Gibco) and ITS+ Premix
634 (Corning), and cultured for 20 hours at 37°C. Cell culture supernatants were then centrifuged

635 at 12000 g for 10 minutes at 4°C, snap frozen in liquid nitrogen, and stored at -80°C until further
636 use.
637 PAMMs were isolated according to a published protocol (Thomas *et al.*, 2021), with some
638 adjustments. Briefly, villi were scraped with a scalpel and digested with 0.2% Trypsin
639 (Invitrogen) and 12.5 mg/ml DNase I (Sigma-Aldrich) in HBSS-Mg/Ca-free medium (Sigma-
640 Aldrich) at 37°C for 7 min. The resulting single cell suspension was passed through a 70 µm
641 cell strainer (Falcon). If necessary, red blood cells were lysed by incubating cells in a buffer
642 containing 155 mM NH4Cl, 10 mM KHCO3, and 0.1 mM EDTA (pH 7.3) for 5 min, before
643 staining for FACS sorting. PAMMs were defined as CD45+HLA-DR+ cells.
644 Primary EVTs were isolated according to a previously published protocol (Haider et al., 2016).
645 Briefly, villi were scraped with a scalpel and digested in two sequential digestion steps using
646 0.125% trypsin (Invitrogen) and 12.5 mg/ml DNase I (Sigma-Aldrich) in HBSS-Mg/Ca-free
647 medium (Sigma-Aldrich). Each digest was performed at 37°C for 30 min without agitation.
648 Subsequently, cells were filtered through a 100 µm cell strainer (Falcon). The cells were then
649 layered on top of a Percoll gradient (10–70%; Pharmacia, Uppsala, Sweden) and centrifuged
650 at 1,175 g at 4°C for 24 min without braking at the end of the run. Cells between 35% and 50%
651 of the Percoll layer were collected. If necessary, red blood cells were lysed by incubating cells
652 in a buffer containing 155 mM NH4Cl, 10 mM KHCO3, and 0.1 mM EDTA (pH 7.3) for 5 min.
653 Remaining cells were then magnetically labeled with HLA-G – PE antibody and anti-PE
654 microbeads and enriched for HLA-G+ EVTs by magnetic-activated cell sorting using an
655 OctoMACS separator and MS columns (Miltenyi Biotec).
656 HLA-G+ EVTs were seeded on fibronectin-coated tissue culture plates (Nunc Cell-Culture
657 Plates, ThermoFisher) at a density of 1 million cells/ml EVT culture medium, consisting of
658 DMEM/F-12, GlutaMAX (Gibco), supplemented with 10% FBS Superior (Sigma Aldrich), 50
659 µg/ml gentamicin (Gibco), and 0.5 µg/mL fungizone (Gibco), and left to differentiate for 1-3
660 days before collecting cell culture supernatants. The conditioned media were centrifuged at
661 12000 g for 10 minutes at 4°C, snap frozen in liquid nitrogen, and stored at -80°C until further
662 use.

663 **Cell density**

664 To determine the density of cells within decidual tissues, the tissue was weighed before
665 digestion and the weight was correlated with the cellular output after digestion, determined by
666 a CASY TT cell counter.

667

668 **Western Blotting**

669 Decidual tissue samples (decB and decP) were selected according to our established tissue
670 sampling protocol described in Fig. S1, A and B. Tissue homogenization, lysis and
671 determination of protein concentration was performed as recently published (Windsperger *et*
672 *al.*, 2020). Briefly, protein concentration was evaluated using a Bradford protein assay
673 (adjusted to 1µg / µl in 1% sodium dodecyl sulphate) and additionally corrected by the
674 evaluation of protein band intensities using a stain-free acrylamide solution (TGX FastCast,
675 Bio-Rad). Prior to blotting bands were visualized by an imaging system (ChemiDoc, Bio-Rad)
676 and band intensities were determined by Image Lab 6.0.1 (Bio-Rad) by calculating the
677 Adjusted Volume (Adj.Vol) of all protein bands visualized. Proteins were then blotted onto
678 polyvinylidene fluoride membranes (GE Healthcare, Buckinghamshire, UK), blocked with
679 skimmed milk and incubated with primary antibodies (Table S1) overnight at 4°C. Finally, blots
680 were incubated with horseradish peroxidase-conjugated secondary antibodies (Table S1).
681 Signals were visualized with ChemiDoc Imaging System (Bio-Rad).

682

683 **Flow cytometry**

684 For analysis of immune cell distributions within decidual tissues, cells were isolated as
685 described above and stained for flow cytometry using the antibodies listed in Table S1. Immune
686 cells were defined as $CD45^{+}$. Within the immune cell gate, neutrophils were defined as
687 $CD66b^{+}$, macrophages/monocytes were defined as $CD66b^{-}CD14^{+}$, dNK/uNK cells were
688 defined as $CD3^{-}CD56^{hi}$, T cells were defined as $CD3^{+}$, and B cells were defined as $CD19^{+}$. All
689 defined immune cell types were mutually exclusive. Measurements were performed using a
690 FACSVerse (BD) and DxFLEX flow cytometer (Beckman Coulter).

691 To create the TSNE plot in Fig. 1 we used the CyTOF workflow as published by Nowicka et al.
692 (Nowicka et al., 2017) and modified it accordingly for flow cytometry data.
693
694 **Immunofluorescence of decidual tissue sections**
695 First trimester decidual tissues were fixed in 7.5% formaldehyde and embedded in paraffin
696 (Merck). Sections (2.5 µm) were cut using a microtome (HM355; Microm) and deparaffinized
697 by incubating for 10 minutes in Xylene, followed by 100%, 96%, and 70% ethanol, and
698 deionized water. Antigens were retrieved using citrate buffer (pH 6.0, Sigma-Aldrich) in a KOS
699 MicrowaveStation (Milestone SRL). When indicated sections were stained with Hematoxylin
700 and Eosin using an automated slide stainer with (Tissue Tek Prisma Plus, Sakura Finetek).
701 For staining, sections were blocked for 1 hour in TBS/T containing 5% normal goat serum (Cell
702 Signaling Technology) and then incubated with primary antibodies listed in Table S1 overnight
703 at 4°C. Subsequently, the slides were washed in TBS/T 3 times and then incubated with
704 secondary antibodies (2 µg/ml) and DAPI (1 µg/ml, Roche) for 1 hour at room temperature.
705 Images were acquired on a fluorescence microscope (Olympus BX50) using a Hamamatsu
706 ORCA-sparc digital camera and the Olympus cellSens Standard software.
707
708 **Explant culture**
709 Explants were generated by cutting decB and decP tissue into small pieces of approximately
710 1x1 cm. Explants were weighed and put into 4 ml of Decidua culture medium per 1 gram of
711 tissue, then cultured overnight at 37°C. Of note, decidual explant cultures have been shown to
712 maintenance high viability over six days *ex vivo*, in culture (Hazan et al., 2010). Conditioned
713 media were centrifuged at 12000 g for 10 minutes at 4°C, snap frozen in liquid nitrogen and
714 stored at -80°C until further use.
715 To assess the effect of EVT-CM on macrophages *in situ*, explants were cultured in 50% EVT-
716 CM overnight, then fixed in 7.5% formaldehyde and processed for immunofluorescence as
717 described above. For proliferation assays, 10 µM EdU (EdU-Click 488 kit, baseclick) was
718 added to the explant culture and the EdU detection protocol was performed according to

719 manufacturer's user manual before blocking. Sections were co-stained with CD14, and
720 macrophage EdU incorporation was assessed using the ImageJ software.
721 For blockage experiments, 1 µg/ml anti-human TGF-β antibody was added to the culture.
722

723 **Analysis of conditioned media**

724 Conditioned media from decB and decP explants were analyzed by the proximity extension
725 assay on the Olink proteomics platform (www.olink.com), using the Inflammation Panel.
726 Samples were sent to and analyzed by the Clinical Biomarker Facility Unit at SciLifeLab in
727 Uppsala, Sweden.
728 Conditioned media from decB and decP explants, as well as decBAMMs, decPAMMs, EVTs,
729 and decB neutrophils, were analyzed using the magnetic bead-based immunoassays by Bio-
730 Techne (Luminex Performance Assay TGF-β Premixed Kit and Luminex Discovery Assay with
731 personalized panels). The samples were processed according to manufacturer's user manual
732 and measured on a Luminex 200 machine.
733

734 **RNA sequencing**

735 After isolation of macrophages or monocytes (as described above), RNA was extracted using
736 the SPLIT RNA Extraction Kit (Lexogen) and sent to Lexogen in Vienna for library preparation
737 and sequencing (QuantSeq). Fastq files were aligned to the human reference genome
738 GRCh38 with Gencode annotation using STAR aligner in 2-pass mode (Dobin et al., 2013).
739 The count matrices were calculated with STAR/htseq-count. Differential gene expression was
740 calculated using DESeq2 (Love et al., 2014) , applying batch modelling where required. Genes
741 with counts lower than 100 in 90% of samples were filtered out. LFC shrinkage with
742 approximate posterior estimation for GLM coefficients was applied for downstream
743 visualization (Zhu et al., 2019) . For the PCA visualization, batch effects were removed with
744 limma (Ritchie et al., 2015). We calculated Gene Ontology enrichment scores with the webtool
745 g:Profiler and plotted the data in R (Ashburner et al., 2000; Gene Ontology, 2021; Reimand et
746 al., 2007).

747 scRNA-seq data were downloaded from EMBL-EBI using the accession number E-MTAB-
748 6701. Raw sequencing data were aligned to the reference genome GRCh38 using 10x
749 Genomics Cell Ranger 6.1.2. Output files were analyzed and filtered with the R package Seurat
750 4.0.6 (Butler et al., 2018; Hao et al., 2021; Satija et al., 2015; Stuart et al., 2019). All cells with
751 low overall gene expression or which showed high mitochondrial gene expression were filtered
752 out. The data were log-normalized before entering the Seurat integration workflow. Cluster
753 annotation was performed applying the list of cluster-specific genes published along with the
754 original publication (Vento-Tormo *et al.*, 2018). Violin plots were created with the Seurat VInplot
755 function, using either single gene expression or module scores, calculated with the Seurat
756 AddModuleScore function (Butler *et al.*, 2018; Hao *et al.*, 2021; Satija *et al.*, 2015; Stuart *et al.*,
757 2019).
758

759 **PBMC migration assay**

760 Blood from healthy, non-pregnant female donors was collected in Na-heparin tubes and
761 PBMCs were isolated using Lymphoprep (Axis Shield) according to manufacturer's instruction.
762 Conditioned media of decB and decP explants were pipetted into wells of a 24-well plate
763 (Corning) at a concentration of 25% CM in Transwell medium consisting of Roswell Park
764 Memorial Institute (RPMI) 1640 medium supplemented with 1 mg/ml human serum albumin
765 (Octapharma), and 100 units/ml penicillin, 100 µg/ml streptomycin and 29.2 mg/ml L-glutamine
766 (Gibco). Transwell inserts (6.5 mm inserts with 5.0 µm pores, Corning) were coated with 1.43
767 mg/ml Matrigel (Growth factor-reduced, Corning) for 1 hour at room temperature. Then, the
768 inserts were placed into the wells containing the CM and the plate was pre-incubated for 1
769 hour at 37°C. PBMCs were seeded into the top part of the transwell insert (0.5 million cells in
770 100 µl Transwell medium) and the plate was incubated at 37°C for 4 hours. Migrated cells were
771 collected by taking up the medium from the bottom part of the transwell and scraping any
772 adherent cells off the bottom of the plate. Cells were then stained for flow cytometry and
773 analyzed using a FACSCanto II flow cytometer (BD). TruCount tubes (BD) were used to
774 determine the absolute numbers of migrated cells.

775

776 **Neutrophil migration assay**

777 Neutrophil migration towards decB and decP supernatants was measured using 96-well trans
778 well plates (Corning, 5 µm polycarbonate membranes). Filters were pre-soaked in buffer (PBS
779 with Ca2+/Mg2+ supplemented with 0.1% BSA, 10 mM HEPES, and 10 mM glucose) for 1 hr
780 at 37°C. Polymorphonuclear leukocytes (PMNLs) were isolated from healthy, non-pregnant
781 donors as previously described (Valadez-Cosmes et al., 2021). Bottom wells were loaded with
782 100 µl supernatants (1:2 dilution with media) and upper wells with 100 µl PMNL (4x106 cell/ml).
783 Cells were allowed to migrate for 1hr at 37°C and subsequently fixed with 150 µl of fixation
784 solution (CellFIX, BD). Number of migrated neutrophils was measured at a BD FACSCanto II
785 for 30 sec and separated from eosinophils based on their different auto-fluorescence in the
786 V450 channel.

787

788 **Cell Tracking**

789 For in vitro analysis of cell motility, macrophages were seeded at a density of 250.000 cells/ml
790 Decidua culture medium and incubated in a Lionheart FX automated live cell imager at 37°C
791 and 5% CO2. Time-lapse videos were created by taking a picture every 5 minutes for 24 hours,
792 using the Gen5 3.08 software. All images between 12 and 24 hours of culture were used to
793 track cells and analyze their speed with the CellTracker tool in MATLAB
794 (http://celltracker.website). Cell starting coordinates were set to 0,0 and subsequent data
795 points were newly calculated accordingly for visualization purposes. Cell tracks were visualized
796 in R.

797

798 **Phagocytosis Assay**

799 Decidual cells were isolated as described above and incubated in the presence of
800 fluorescence-labeled latex beads (50 beads per cell; latex beads, 1 µm, carboxylate-modified
801 polystyrene, fluorescent yellow-green, Merck) for 2 hours at 37°C. A negative control was
802 incubated for 2 hours at 4°C to control for non-specific adhesion of beads to the cell surface.

803 Then, cells were detached from the plate using Accutase (Gibco StemPro Accutase, Fisher
804 Scientific) and stained for flow cytometry. Phagocytosis was assessed on a FACSVerse flow
805 cytometer using the BD FACSuite software, by measuring the signal of the beads within the
806 macrophage gate (using the negative control as a gate-setting control).
807 To measure the effect of EVT-CM on macrophage phagocytosis, the cells were cultured in
808 50% EVT-CM. For blockage experiments, 1 µg/ml anti-human TGF-β or 20 µg/ml anti-human
809 PD-L1 antibody was added to the culture.
810

811 **T cell assays**

812 T cells were isolated from PBMC of healthy, non-pregnant female volunteers using the Pan T
813 Cell Isolation Kit (Miltenyi,130-096-535). To monitor proliferation, T cells were labeled with 5
814 µM carboxyfluorescein diacetate succinimidyl (CFSE Cell Division Tracker Kit, Biolegend). For
815 Treg induction and T cell activation, flat-bottomed 96-well plates (Nunc Cell-Culture Plates,
816 ThermoFisher) were coated with 1 µg/ml anti-CD3 and 2 µg/ml anti-CD28 antibodies
817 (BioLegend) for 2 hours and seeded with 50.000 T cells/well. To measure the effect of
818 macrophages and EVT-CM on T cell proliferation and Treg induction, 5.000 macrophages
819 and/or 50% EVT-CM were added to the culture. For the blockage experiments, 1 µg/ml anti-
820 human TGF-β antibody was added to the co-culture. After three days, T cell proliferation was
821 determined by CFSE dilution and Treg differentiation was determined by surface staining of
822 CD25 and intracellular staining of FOXP3 using the eBioscience Foxp3/Transcription Factor
823 staining buffer set (Invitrogen). Data were collected using a FACSVerse flow cytometer using
824 the BD FACSuite software and were analyzed with FlowJo 10.7.
825

826 **Accession codes and data availability**

827 BioProject accession number for RNA-seq of isolated samples: GSE196917
828

829 **Acknowledgments**

830 We thank all patients and staff at Gynmed Clinic (Vienna) for providing placental and decidual
831 samples. We thank the FACS Core Unit at the St. Anna Children's Cancer Research Institute
832 (Vienna) and Boris Kovacic and Dieter Printz (St. Anna Children's Cancer Research Institute
833 Vienna) are greatly acknowledged for technical help and advices with flow cytometry-based
834 analysis and sorting. Emir Hadzijusufovic (Division of Hematology and Hemostaseology,
835 Department of Internal Medicine I, Medical University of Vienna) is acknowledged for technical
836 help with cell staining. The authors would like to acknowledge support of the Clinical biomarker
837 facility at SciLifeLab Sweden for providing assistance in protein analyses. We thank Benjamin
838 Schuster (Vienna University of Technology) for his help with computational analysis. Thomas
839 Weichhart (Center of Pathobiochemistry and Genetics, Institute of Medical Genetics, Medical
840 University of Vienna, Vienna) is acknowledged for scientific discussion.
841 This work was supported by the Austrian Science Fund (P33485 to J.P.) and by the Austrian
842 National Bank (17613ONB to J.P.).
843

844 **Author contributions**

845 Conceptualization, J. Pollheimer, S. Vondra, A.L. Höbler, A.I. Lackner, R. Bauer, J. Kargl, J.,
846 G. Schabbauer, Ernerudh. Formal analysis, J. Pollheimer, S. Vondra, A.L. Höbler, A.I. Lackner,
847 J. Raffetseder, Z.N. Mihalic, V. Kunihs, P. Haslinger, S. Haider, J. Kargl, H. Husslein. Funding
848 acquisition, J. Pollheimer. Methodology, J. Pollheimer, S. Vondra, A.L. Höbler, A.I. Lackner, J.
849 Raffetseder, A. Vogel, S. Haider, R. Oberle, M. Wahrmann, J. Ernerudh, J. Kargl. Intellectual
850 input, J. Pollheimer, S. Vondra, A.L. Höbler, A.I. Lackner, J. Raffetseder, A. Vogel, L. Saleh,
851 S. Haider, M. Wahrmann, R. Bauer, J. Kargl, H. Husslein, P. Latos, G. Schabbauer, M. Knöfler,
852 J. Ernerudh. Supervision, J. Pollheimer. Visualization, J. Pollheimer, S. Vondra, A.L. Höbler,
853 A.I. Lackner. Writing, J. Pollheimer, S. Vondra, A.L. Höbler, A.I. Lackner.
854

855 All authors discussed the manuscript.
856

857 **Competing Interests**

Disclosures: The authors declare no competing interests exist.

References

Abbas, Y., Carnicer-Lombarte, A., Gardner, L., Thomas, J., Brosens, J.J., Moffett, A., Sharkey, A.M., Franze, K., Burton, G.J., and Oyen, M.L. (2019). Tissue stiffness at the human maternal-fetal interface. Hum Reprod *34*, 1999-2008. 10.1093/humrep/dez139.

Allenspach, E.J., Lemos, M.P., Porrett, P.M., Turka, L.A., and Laufer, T.M. (2008). Migratory and lymphoid-resident dendritic cells cooperate to efficiently prime naive CD4 T cells. Immunity *29*, 795-806. 10.1016/j.immuni.2008.08.013.

Amsalem, H., Kwan, M., Hazan, A., Zhang, J., Jones, R.L., Whittle, W., Kingdom, J.C., Croy, B.A., Lye, S.J., and Dunk, C.E. (2014). Identification of a novel neutrophil population: proangiogenic granulocytes in second-trimester human decidua. J Immunol *193*, 3070-3079. 10.4049/jimmunol.1303117.

Ardi, V.C., Kupriyanova, T.A., Deryugina, E.I., and Quigley, J.P. (2007). Human neutrophils uniquely release TIMP-free MMP-9 to provide a potent catalytic stimulator of angiogenesis. Proc Natl Acad Sci U S A *104*, 20262-20267. 10.1073/pnas.0706438104.

Ashburner, M., Ball, C.A., Blake, J.A., Botstein, D., Butler, H., Cherry, J.M., Davis, A.P., Dolinski, K., Dwight, S.S., Eppig, J.T., et al. (2000). Gene ontology: tool for the unification of biology. The Gene Ontology Consortium. Nat Genet *25*, 25-29. 10.1038/75556.

Bajpai, G., Schneider, C., Wong, N., Bredemeyer, A., Hulsmans, M., Nahrendorf, M., Epelman, S., Kreisel, D., Liu, Y., Itoh, A., et al. (2018). The human heart contains distinct macrophage subsets with divergent origins and functions. Nat Med *24*, 1234-1245. 10.1038/s41591-018-0059-x.

Bekes, E.M., Schweighofer, B., Kupriyanova, T.A., Zajac, E., Ardi, V.C., Quigley, J.P., and Deryugina, E.I. (2011). Tumor-recruited neutrophils and neutrophil TIMP-free MMP-9 regulate coordinately the levels of tumor angiogenesis and efficiency of malignant cell intravasation. Am J Pathol *179*, 1455-1470. 10.1016/j.ajpath.2011.05.031.

Bittmann, I., Dose, T., Baretton, G.B., Muller, C., Schwaiblmair, M., Kur, F., and Lohrs, U. (2001). Cellular chimerism of the lung after transplantation. An interphase cytogenetic study. Am J Clin Pathol *115*, 525-533. 10.1309/GAFN-5MPA-LY8E-DTPQ.

Bronte, V., Brandau, S., Chen, S.H., Colombo, M.P., Frey, A.B., Greten, T.F., Mandruzzato, S., Murray, P.J., Ochoa, A., Ostrand-Rosenberg, S., et al. (2016). Recommendations for myeloid-derived suppressor cell nomenclature and characterization standards. Nat Commun *7*, 12150. 10.1038/ncomms12150.

Brosens, I., Pijnenborg, R., Vercruysse, L., and Romero, R. (2011). The "Great Obstetrical Syndromes" are associated with disorders of deep placentation. Am J Obstet Gynecol *204*, 193-201. 10.1016/j.ajog.2010.08.009.

Bulmer, J.N., Morrison, L., Longfellow, M., Ritson, A., and Pace, D. (1991). Granulated lymphocytes in human endometrium: histochemical and immunohistochemical studies. Hum Reprod *6*, 791-798. 10.1093/oxfordjournals.humrep.a137430.

Butler, A., Hoffman, P., Smibert, P., Papalexi, E., and Satija, R. (2018). Integrating single-cell transcriptomic data across different conditions, technologies, and species. Nat Biotechnol *36*, 411-420. 10.1038/nbt.4096.

Byrne, A.J., Powell, J.E., O'Sullivan, B.J., Ogger, P.P., Hoffland, A., Cook, J., Bonner, K.L., Hewitt, R.J., Wolf, S., Ghai, P., et al. (2020). Dynamics of human monocytes and airway macrophages during healthy aging and after transplant. J Exp Med *217*. 10.1084/jem.20191236.

Celada, A., and Maki, R.A. (1992). Transforming growth factor-beta enhances the M-CSF and GM-CSF-stimulated proliferation of macrophages. J Immunol *148*, 1102-1105.

Chaouat, G., Assal Meliani, A., Martal, J., Raghupathy, R., Elliott, J.F., Mosmann, T., and Wegmann, T.G. (1995). IL-10 prevents naturally occurring fetal loss in the CBA x DBA/2 mating combination, and local defect in IL-10 production in this abortion-prone combination is corrected by in vivo injection of IFN-tau. J Immunol *154*, 4261-4268.

Croxatto, D., Micheletti, A., Montaldo, E., Orecchia, P., Loiacono, F., Canegallo, F., Calzetti, F., Fulcheri, E., Munari, E., Zamo, A., et al. (2016). Group 3 innate lymphoid cells regulate neutrophil migration and function in human decidua. Mucosal Immunol *9*, 1372-1383. 10.1038/mi.2016.10.

Dobin, A., Davis, C.A., Schlesinger, F., Drenkow, J., Zaleski, C., Jha, S., Batut, P., Chaisson, M., and Gingeras, T.R. (2013). STAR: ultrafast universal RNA-seq aligner. Bioinformatics *29*, 15-21. 10.1093/bioinformatics/bts635.

Erlebacher, A. (2013). Immunology of the maternal-fetal interface. Annu Rev Immunol *31*, 387-411. 10.1146/annurev-immunol-032712-100003.

Fan, X., Rai, A., Kambham, N., Sung, J.F., Singh, N., Petitt, M., Dhal, S., Agrawal, R., Sutton, R.E., Druzin, M.L., et al. (2014). Endometrial VEGF induces placental sFLT1 and leads to pregnancy complications. J Clin Invest *124*, 4941-4952. 10.1172/JCI76864.

Gautier, E.L., Shay, T., Miller, J., Greter, M., Jakubzick, C., Ivanov, S., Helft, J., Chow, A., Elpek, K.G., Gordonov, S., et al. (2012). Gene-expression profiles and transcriptional regulatory pathways that underlie the identity and diversity of mouse tissue macrophages. Nat Immunol *13*, 1118-1128. 10.1038/ni.2419.

Gene Ontology, C. (2021). The Gene Ontology resource: enriching a GOld mine. Nucleic Acids Res *49*, D325-D334. 10.1093/nar/gkaa1113.

Ginhoux, F., Greter, M., Leboeuf, M., Nandi, S., See, P., Gokhan, S., Mehler, M.F., Conway, S.J., Ng, L.G., Stanley, E.R., et al. (2010). Fate mapping analysis reveals that adult microglia derive from primitive macrophages. Science *330*, 841-845. 10.1126/science.1194637.

Ginhoux, F., and Guilliams, M. (2016). Tissue-Resident Macrophage Ontogeny and Homeostasis. Immunity *44*, 439-449. 10.1016/j.immuni.2016.02.024.

Gordon, S.R., Maute, R.L., Dulken, B.W., Hutter, G., George, B.M., McCracken, M.N., Gupta, R., Tsai, J.M., Sinha, R., Corey, D., et al. (2017). PD-1 expression by tumour-associated macrophages inhibits phagocytosis and tumour immunity. Nature *545*, 495-499. 10.1038/nature22396.

Haider, S., Meinhardt, G., Saleh, L., Fiala, C., Pollheimer, J., and Knofler, M. (2016). Notch1 controls development of the extravillous trophoblast lineage in the human placenta. Proc Natl Acad Sci U S A *113*, E7710-E7719. 10.1073/pnas.1612335113.

Haller, H., Tedesco, F., Rukavina, D., Radillo, O., Gudelj, L., and Beer, A.E. (1995). Decidual-trophoblast interactions: decidual lymphoid cell populations in basal and parietal decidua. J Reprod Immunol *28*, 165-171. 10.1016/0165-0378(94)00913-r.

Hamilton, G.S., Lysiak, J.J., Watson, A.J., and Lala, P.K. (1998). Effects of colony stimulating factor-1 on human extravillous trophoblast growth and invasion. J Endocrinol *159*, 69-77. 10.1677/joe.0.1590069.

Hao, Y., Hao, S., Andersen-Nissen, E., Mauck, W.M., 3rd, Zheng, S., Butler, A., Lee, M.J., Wilk, A.J., Darby, C., Zager, M., et al. (2021). Integrated analysis of multimodal single-cell data. Cell *184*, 3573-3587 e3529. 10.1016/j.cell.2021.04.048.

Hazan, A.D., Smith, S.D., Jones, R.L., Whittle, W., Lye, S.J., and Dunk, C.E. (2010). Vascular-leukocyte interactions: mechanisms of human decidual spiral artery remodeling in vitro. Am J Pathol *177*, 1017-1030. 10.2353/ajpath.2010.091105.

Helige, C., Ahammer, H., Moser, G., Hammer, A., Dohr, G., Huppertz, B., and Sedlmayr, P. (2014). Distribution of decidual natural killer cells and macrophages in the neighbourhood of the trophoblast invasion front: a quantitative evaluation. Hum Reprod *29*, 8-17. 10.1093/humrep/det353.

Hiby, S.E., Apps, R., Sharkey, A.M., Farrell, L.E., Gardner, L., Mulder, A., Claas, F.H., Walker, J.J., Redman, C.W., Morgan, L., et al. (2010). Maternal activating KIRs protect against human reproductive failure mediated by fetal HLA-C2. J Clin Invest *120*, 4102-4110. 10.1172/JCI43998.

Houser, B.L., Tilburgs, T., Hill, J., Nicotra, M.L., and Strominger, J.L. (2011). Two unique human decidual macrophage populations. J Immunol *186*, 2633-2642. 10.4049/jimmunol.1003153.

Itano, A.A., McSorley, S.J., Reinhardt, R.L., Ehst, B.D., Ingulli, E., Rudensky, A.Y., and Jenkins, M.K. (2003). Distinct dendritic cell populations sequentially present antigen to CD4 T cells and stimulate different aspects of cell-mediated immunity. Immunity *19*, 47-57. 10.1016/s1074-7613(03)00175-4.

Klein, I., Cornejo, J.C., Polakos, N.K., John, B., Wuensch, S.A., Topham, D.J., Pierce, R.H., and Crispe, I.N. (2007). Kupffer cell heterogeneity: functional properties of bone marrow derived and sessile hepatic macrophages. Blood *110*, 4077-4085. 10.1182/blood-2007-02-073841.

Knofler, M., Haider, S., Saleh, L., Pollheimer, J., Gamage, T., and James, J. (2019). Human placenta and trophoblast development: key molecular mechanisms and model systems. Cell Mol Life Sci *76*, 3479-3496. 10.1007/s00018-019-03104-6.

Kolaczkowska, E., and Kubes, P. (2013). Neutrophil recruitment and function in health and inflammation. Nat Rev Immunol *13*, 159-175. 10.1038/nri3399.

Lindau, R., Vondra, S., Spreckels, J., Solders, M., Svensson-Arvelund, J., Berg, G., Pollheimer, J., Kaipe, H., Jenmalm, M.C., and Ernerudh, J. (2021). Decidual stromal cells support tolerance at the human foetal-maternal interface by inducing regulatory M2 macrophages and regulatory T-cells. J Reprod Immunol *146*, 103330. 10.1016/j.jri.2021.103330.

Love, M.I., Huber, W., and Anders, S. (2014). Moderated estimation of fold change and dispersion for RNA-seq data with DESeq2. Genome Biol *15*, 550. 10.1186/s13059-014-0550-8.

McGovern, N., Schlitzer, A., Gunawan, M., Jardine, L., Shin, A., Poyner, E., Green, K., Dickinson, R., Wang, X.N., Low, D., et al. (2014). Human dermal CD14(+) cells are a transient population of monocyte-derived macrophages. Immunity *41*, 465-477. 10.1016/j.immuni.2014.08.006.

Moffett, A., Chazara, O., and Colucci, F. (2017). Maternal allo-recognition of the fetus. Fertil Steril *107*, 1269-1272. 10.1016/j.fertnstert.2017.05.001.

Murphy, S.P., Fast, L.D., Hanna, N.N., and Sharma, S. (2005). Uterine NK cells mediate inflammation-induced fetal demise in IL-10-null mice. J Immunol *175*, 4084-4090. 10.4049/jimmunol.175.6.4084.

Nancy, P., Tagliani, E., Tay, C.S., Asp, P., Levy, D.E., and Erlebacher, A. (2012). Chemokine gene silencing in decidual stromal cells limits T cell access to the maternal-fetal interface. Science *336*, 1317-1321. 10.1126/science.1220030.

Nath, M.C., Cubro, H., McCormick, D.J., Milic, N.M., and Garovic, V.D. (2020). Preeclamptic Women Have Decreased Circulating IL-10 (Interleukin-10) Values at the Time of Preeclampsia Diagnosis: Systematic Review and Meta-Analysis. Hypertension *76*, 1817-1827. 10.1161/HYPERTENSIONAHA.120.15870.

981 Nowicka, M., Krieg, C., Crowell, H.L., Weber, L.M., Hartmann, F.J., Guglietta, S., Becher, B., Levesque, M.P.,
982 and Robinson, M.D. (2017). CyTOF workflow: differential discovery in high-throughput high-dimensional
983 cytometry datasets. F1000Res *6*, 748. 10.12688/f1000research.11622.3.
984 Okabe, Y., and Medzhitov, R. (2014). Tissue-specific signals control reversible program of localization and
985 functional polarization of macrophages. Cell *157*, 832-844. 10.1016/j.cell.2014.04.016.
986 Palis, J., Robertson, S., Kennedy, M., Wall, C., and Keller, G. (1999). Development of erythroid and myeloid
987 progenitors in the yolk sac and embryo proper of the mouse. Development *126*, 5073-5084.
988 10.1242/dev.126.22.5073.
989 Plaisier, M., Rodrigues, S., Willems, F., Koolwijk, P., van Hinsbergh, V.W., and Helmerhorst, F.M. (2007).
990 Different degrees of vascularization and their relationship to the expression of vascular endothelial growth factor,
991 placental growth factor, angiopoietins, and their receptors in first-trimester decidual tissues. Fertil Steril *88*, 176-
992 187. 10.1016/j.fertnstert.2006.11.102.
993 Pollheimer, J., Vondra, S., Baltayeva, J., Beristain, A.G., and Knofler, M. (2018). Regulation of Placental
994 Extravillous Trophoblasts by the Maternal Uterine Environment. Front Immunol *9*, 2597.
995 10.3389/fimmu.2018.02597.
996 Reimand, J., Kull, M., Peterson, H., Hansen, J., and Vilo, J. (2007). g:Profiler--a web-based toolset for functional
997 profiling of gene lists from large-scale experiments. Nucleic Acids Res *35*, W193-200. 10.1093/nar/gkm226.
998 Repnik, U., Tilburgs, T., Roelen, D.L., van der Mast, B.J., Kanhai, H.H., Scherjon, S., and Claas, F.H. (2008).
999 Comparison of macrophage phenotype between decidua basalis and decidua parietalis by flow cytometry. Placenta
1000 *29*, 405-412. 10.1016/j.placenta.2008.02.004.
1001 Ritchie, M.E., Phipson, B., Wu, D., Hu, Y., Law, C.W., Shi, W., and Smyth, G.K. (2015). limma powers
1002 differential expression analyses for RNA-sequencing and microarray studies. Nucleic Acids Res *43*, e47.
1003 10.1093/nar/gkv007.
1004 Rizzuto, G., Brooks, J.F., Tuomivaara, S.T., McIntyre, T.I., Ma, S., Rideaux, D., Zikherman, J., Fisher, S.J., and
1005 Erlebacher, A. (2022). Establishment of fetomaternal tolerance through glycan-mediated B cell suppression.
1006 Nature *603*, 497-502. 10.1038/s41586-022-04471-0.
1007 Ruffell, B., and Coussens, L.M. (2015). Macrophages and therapeutic resistance in cancer. Cancer Cell *27*, 462-
1008 472. 10.1016/j.ccell.2015.02.015.
1009 Salvany-Celades, M., van der Zwan, A., Benner, M., Setrajcic-Dragos, V., Bougleux Gomes, H.A., Iyer, V.,
1010 Norwitz, E.R., Strominger, J.L., and Tilburgs, T. (2019). Three Types of Functional Regulatory T Cells Control T
1011 Cell Responses at the Human Maternal-Fetal Interface. Cell Rep *27*, 2537-2547 e2535.
1012 10.1016/j.celrep.2019.04.109.
1013 Satija, R., Farrell, J.A., Gennert, D., Schier, A.F., and Regev, A. (2015). Spatial reconstruction of single-cell gene
1014 expression data. Nat Biotechnol *33*, 495-502. 10.1038/nbt.3192.
1015 Solders, M., Gorchs, L., Gidlof, S., Tiblad, E., Lundell, A.C., and Kaipe, H. (2017). Maternal Adaptive Immune
1016 Cells in Decidua Parietalis Display a More Activated and Coinhibitory Phenotype Compared to Decidua Basalis.
1017 Stem Cells Int *2017*, 8010961. 10.1155/2017/8010961.
1018 Stuart, T., Butler, A., Hoffman, P., Hafemeister, C., Papalexi, E., Mauck, W.M., 3rd, Hao, Y., Stoeckius, M.,
1019 Smibert, P., and Satija, R. (2019). Comprehensive Integration of Single-Cell Data. Cell *177*, 1888-1902 e1821.
1020 10.1016/j.cell.2019.05.031.
1021 Svensson-Arvelund, J., Mehta, R.B., Lindau, R., Mirrasekhian, E., Rodriguez-Martinez, H., Berg, G., Lash, G.E.,
1022 Jenmalm, M.C., and Ernerudh, J. (2015). The human fetal placenta promotes tolerance against the semiallogeneic
1023 fetus by inducing regulatory T cells and homeostatic M2 macrophages. J Immunol *194*, 1534-1544.
1024 10.4049/jimmunol.1401536.
1025 Svensson, J., Jenmalm, M.C., Matussek, A., Geffers, R., Berg, G., and Ernerudh, J. (2011). Macrophages at the
1026 fetal-maternal interface express markers of alternative activation and are induced by M-CSF and IL-10. J Immunol
1027 *187*, 3671-3682. 10.4049/jimmunol.1100130.
1028 Tamoutounour, S., Guilliams, M., Montanana Sanchis, F., Liu, H., Terhorst, D., Malosse, C., Pollet, E., Ardouin,
1029 L., Luche, H., Sanchez, C., et al. (2013). Origins and functional specialization of macrophages and of conventional
1030 and monocyte-derived dendritic cells in mouse skin. Immunity *39*, 925-938. 10.1016/j.immuni.2013.10.004.
1031 Thomas, J.R., Appios, A., Zhao, X., Dutkiewicz, R., Donde, M., Lee, C.Y.C., Naidu, P., Lee, C., Cerveira, J., Liu,
1032 B., et al. (2021). Phenotypic and functional characterization of first-trimester human placental macrophages,
1033 Hofbauer cells. J Exp Med *218*. 10.1084/jem.20200891.
1034 Tilburgs, T., Evans, J.H., Crespo, A.C., and Strominger, J.L. (2015). The HLA-G cycle provides for both NK
1035 tolerance and immunity at the maternal-fetal interface. Proc Natl Acad Sci U S A *112*, 13312-13317.
1036 10.1073/pnas.1517724112.
1037 Tseng, D., Volkmer, J.P., Willingham, S.B., Contreras-Trujillo, H., Fathman, J.W., Fernhoff, N.B., Seita, J., Inlay,
1038 M.A., Weiskopf, K., Miyanishi, M., and Weissman, I.L. (2013). Anti-CD47 antibody-mediated phagocytosis of
1039 cancer by macrophages primes an effective antitumor T-cell response. Proc Natl Acad Sci U S A *110*, 11103-
1040 11108. 10.1073/pnas.1305569110.
1041 Valadez-Cosmes, P., Maitz, K., Kindler, O., Raftopoulou, S., Kienzl, M., Santiso, A., Mihalic, Z.N., Brcic, L.,
1042 Lindenmann, J., Fediuk, M., et al. (2021). Identification of Novel Low-Density Neutrophil Markers Through

Unbiased High-Dimensional Flow Cytometry Screening in Non-Small Cell Lung Cancer Patients. Front Immunol *12*, 703846. 10.3389/fimmu.2021.703846.

van de Laar, L., Saelens, W., De Prijck, S., Martens, L., Scott, C.L., Van Isterdael, G., Hoffmann, E., Beyaert, R., Saeys, Y., Lambrecht, B.N., and Guilliams, M. (2016). Yolk Sac Macrophages, Fetal Liver, and Adult Monocytes Can Colonize an Empty Niche and Develop into Functional Tissue-Resident Macrophages. Immunity *44*, 755-768. 10.1016/j.immuni.2016.02.017.

Vento-Tormo, R., Efremova, M., Botting, R.A., Turco, M.Y., Vento-Tormo, M., Meyer, K.B., Park, J.E., Stephenson, E., Polanski, K., Goncalves, A., et al. (2018). Single-cell reconstruction of the early maternal-fetal interface in humans. Nature *563*, 347-353. 10.1038/s41586-018-0698-6.

Windsperger, K., Vondra, S., Lackner, A.I., Kunihs, V., Haslinger, P., Meinhardt, G., Dietrich, B., Dekan, S., Fiala, C., Knofler, M., et al. (2020). Densities of decidual high endothelial venules correlate with T-cell influx in healthy pregnancies and idiopathic recurrent pregnancy losses. Hum Reprod *35*, 2467-2477. 10.1093/humrep/deaa234.

Xue, J., Schmidt, S.V., Sander, J., Draffehn, A., Krebs, W., Quester, I., De Nardo, D., Gohel, T.D., Emde, M., Schmidleithner, L., et al. (2014). Transcriptome-based network analysis reveals a spectrum model of human macrophage activation. Immunity *40*, 274-288. 10.1016/j.immuni.2014.01.006.

Zenz, R., Eferl, R., Kenner, L., Florin, L., Hummerich, L., Mehic, D., Scheuch, H., Angel, P., Tschachler, E., and Wagner, E.F. (2005). Psoriasis-like skin disease and arthritis caused by inducible epidermal deletion of Jun proteins. Nature *437*, 369-375. 10.1038/nature03963.

Zhao, H., Kalish, F., Schulz, S., Yang, Y., Wong, R.J., and Stevenson, D.K. (2015). Unique roles of infiltrating myeloid cells in the murine uterus during early to midpregnancy. J Immunol *194*, 3713-3722. 10.4049/jimmunol.1401930.

Zhu, A., Ibrahim, J.G., and Love, M.I. (2019). Heavy-tailed prior distributions for sequence count data: removing the noise and preserving large differences. Bioinformatics *35*, 2084-2092. 10.1093/bioinformatics/bty895.

1069 **Supplementary Data**

1070

1071 **Fig. S1** presents a schematic illustrating how decidual samples were processed for
1072 characterization, their cellular densities after enzymatic digestion, and the characterization of
1073 decidual neutrophils. **Fig. S3** shows representative flow cytometry gating strategies. Fig. S3
1074 shows the characterization of tissue-resident macrophages in decB and decP samples. **Fig.**
1075 **S4** shows the data for chemoattractant assays performed with decB- and decP-CMs using
1076 PBMCs and low magnification IF stainings of proliferative decBAMs. **Fig. S5** represents PCA
1077 and gene set enrichment analysis of RNA-seq data, comparative computational analyses, and
1078 single channel IF stainings of $CD14^+$ decidual macrophages double positive for HMOX1 or
1079 CD44. **Fig. S6** shows the secretome of decidual explants and neutrophils. **Fig. S7** shows
1080 single channel and lower magnification pictures of CD14/CD11c and CD14/HLA-DRA co-
1081 stainings and transcript levels of ITGAX and HLA class II molecules in decBAMs and
1082 decPAMs. **Data S1** presents the complete list of measured factors by the Olink proteomics
1083 platform (related to Fig. 1, D). **Table S1** provides a list of antibodies used in this study.

1084

1085

1086

1087

1088

1089

1090

1091

1092

1093